Biochemistry

pubs.acs.org/biochemistry Article

Peripheral Methionine Residues Impact Flavin Photoreduction and Protonation in an Engineered LOV Domain Light Sensor

Estella F. Yee, Sabine Oldemeyer, Elena Böhm, Abir Ganguly, Darrin M. York, Tilman Kottke, and Brian R. Crane*

Cite This: *Biochemistry* 2021, 60, 1148−1164 Read Online

ACCESS | Metrics & More | Article Recommendations | Supporting Information

ABSTRACT: Proton-coupled electron transfer reactions play critical roles in many aspects of sensory phototransduction. In the case of flavoprotein light sensors, reductive quenching of flavin excited states initiates chemical and conformational changes that ultimately transmit light signals to downstream targets. These reactions generally require neighboring aromatic residues and proton-donating side chains for rapid and coordinated electron and proton transfer to flavin. Although photoreduction of flavoproteins can produce either the anionic (ASQ) or neutral semiquinone (NSQ), the factors that favor one over the other are not well understood. Here we employ a biologically active variant of the light-oxygen-voltage (LOV) domain protein VVD devoid of the adduct-forming Cys residue (VVD-III) to probe the mechanism of flavin photoreduction and protonation. A series of isosteric and conservative residue replacements studied by rate measurements, fluorescence quantum yields, FTIR difference spectroscopy, and molecular dynamics simulations indicate that tyrosine residues facilitate charge recombination reactions that limit sustained flavin reduction, whereas methionine residues facilitate radical propagation and quenching and also gate solvent access for flavin protonation. Replacement of a single surface Met residue with Leu favors formation of the ASQ over the NSQ and desensitizes photoreduction to oxidants. In contrast, increasing site hydrophilicity by Gln substitution promotes rapid NSQ formation and weakens the influence of the redox environment. Overall, the photoreactivity of VVD-III can be understood in terms of redundant electron donors, internal hole quenching, and coupled proton transfer reactions that all depend upon protein conformation, dynamics, and solvent penetration.

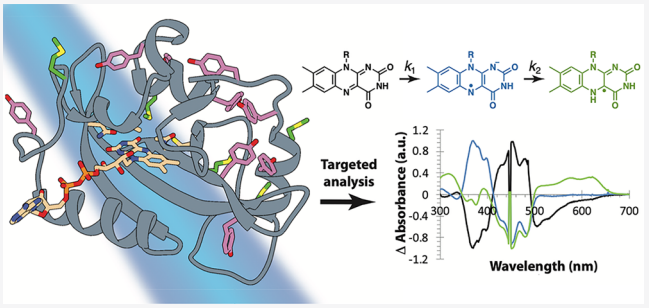

Photochemical reactions of flavins are of long-standing interest owing to their prevalence in important biological processes, including plant light responses (phototropism, stomatal opening, chloroplast movement, and photomorphogenesis[1−4]), environmental stress signaling,[5,6] DNA repair,[7,8] phototaxis,[9,10] and circadian clock regulation.[11,12] Blue light-sensing photoreceptors [cryptochrome/photolyases, light-oxygen-voltage (LOV) domains, and blue light sensor-using FAD (BLUF) domains] couple extrinsic UV/blue light signals to conformational changes and downstream signal transduction through the excitation and reduction of flavin cofactors.[13,14]

Oxidation of redox-active residues allows for the rapid reduction of adjacent flavin cofactors.[13−17] Such light-induced transitions among flavin redox states instigate protein conformational changes through a variety of mechanisms that can involve altered electrostatic interactions with the resulting flavin semiquinone (SQ)[18,19] or modifications to hydrogen-bonding networks between the isoalloxazine ring and adjacent side chains.[20−22] Local interactions propagate to distal positions to release flexible regions, change the oligomeric state, alter protein−protein interactions, and activate effector domains.[23−27]

In LOV domains, signal initiation involves photochemical generation of a flavin-(C4a)-cysteinyl adduct.[28,29] Initial studies suggested a mechanism of adduct formation involving proton transfer (PT) followed by attack on the flavin by the resulting thiolate;[28,29] however, subsequent time-resolved infrared (IR) spectroscopy ruled against an ionic intermediate.[30,31] More recently, spectroscopy and computation on various LOV domains indicate that the reaction could involve electron transfer (ET) followed by PT, hydrogen atom transfer, or highly concerted bond formation.[32−38] Given the importance of proton-coupled electron transfer (PCET) in all of these mechanisms, LOV domains with the adduct-forming cysteine replaced by other nonreactive residues have been extensively studied for their ability to undergo photoinduced flavin reduction.[37,39−45] In most cases, the neutral semiquinone

Received: January 23, 2021
Revised: March 23, 2021
Published: March 31, 2021

https://doi.org/10.1021/acs.biochem.1c00064
Biochemistry 2021, 60, 1148−1164

(NSQ) is the kinetically favored product, although there has been evidence for both stable[42] and transient[37,39] anionic semiquinone (ASQ) radicals. In these processes, the identities of internal protein-based electron donors to the flavin excited state have not been well established. Trp residues, when present, have been suggested as likely candidates,[42] although where examined, spectra of transient radical species have been inconsistent with Trp and challenging to assign.[41] In addition to the semiquinones formed by photoreduction of Cys-less LOV domains, external reductants also produce the doubly reduced hydroquinone (HQ) in some LOV proteins.[44,45]

Unlike photoinduced formation of the ASQ species, photoreduction to the NSQ and to the HQ requires coordinated ET and PT. In LOV domains, the proximal conserved cysteine residue participates in both processes to generate the cysteinyl−thioether covalent bond.[28,46−48] More often, PCET in proteins is multisite in that the transferred proton and electron have different sources.[49] High-potential centers, such as flavin excited states (>2.0 eV),[50,51] can oxidize neighboring tyrosine or tryptophan relay residues (formal potentials of ∼1 eV[52,53]) in electron hole hopping reactions.[54−58] Glycine, polyproline, phenylalanine, and methionine residues have additionally been identified as relay "hopping" centers in small peptide studies.[59−64] However, of these residues, only glycyl radicals are routinely observed to play key roles in protein ET mechanisms.[65−68] Methionine side chains are readily oxidized, but their radical states are unstable, leading to further reactions with oxygen; hence, oxidized Met residues often require methionine sulfoxide reductase for reduction.[69−71] As such, Met residues have been demonstrated only to act as reversible hopping sites in computational studies or in model peptides.[59,60,72] Rapid proton transfer, on the contrary, can occur by acidic side chains and even water molecules but is also highly dependent on the immediate environment.[49] For instance, flavin N5 is protonated by a proximal aspartic acid in plant cryptochrome, whereas the corresponding aspartate in photolyases acts as only a facilitator for proton transfer.[73−75] Alternately, water molecules have been demonstrated to tune the lifetime of photocycles through N5 deprotonation. These water clusters are permitted into the flavin binding pocket through a gating asparagine residue in *Avena sativa* LOV2[76−79] and a threonine residue in *Trichoderma reesei* ENVOY.[80] Because of the complexity of electron and proton transfer in proteins, rational design of such systems is not straightforward. Conversion of the ASQ species of *Escherichia coli* DNA photolyase to the NSQ was attempted by introduction of an aspartate residue analogous to that in NSQ-forming plant cryptochrome; however, the single-residue change did not result in appreciable NSQ formation,[81] likely owing to the lack of stabilization of a protonated aspartic acid as a proton donor. In contrast, a Cys416Asn substitution in *Drosophila* cryptochrome does facilitate ASQ protonation,[82,83] but an increased degree of conversion is observed only when accompanied by an additional Leu405Glu substitution at the protein surface to facilitate proton transport from the bulk to the flavin binding pocket.[83]

Many biological reactions rely on tightly controlled PCET, and as such, investigating the underlying regulation of these reactions can prove illustrative for protein engineering. In previous studies, we manipulated the native PCET reaction of the canonical LOV domain protein VVD by substituting the conserved adduct-forming cysteine residue with a redox-inactive alanine, resulting in NSQ formation upon light excitation.[45,84] Such a strategy has also been implemented in the development of mini singlet oxygen generator proteins (miniSOG) and other singlet oxygen photosensitizing proteins (SOPP) to avoid deactivation of the flavin triplet species by competing electron donation from amino acids[85−89] along with further removal of hydrogen-bonding amino acids to reduce the electron affinity of flavin.[90,91]

Unlike SOPPs, the modified VVD variant retained biological activity because flavin photoreduction occurs in sufficient yield and produces a change in N5 protonation similar to that found in adduct formation.[45,92] Nonetheless, biological activity depends on reductants to donate electrons to the cofactor. Herein, we seek to identify these moieties and better characterize the photoreduction process in the model VVD-III protein by using the spectral sensitivity of the isoalloxazine ring as a useful handle for tracking both ET and PT. We find that redox-active aromatic side chains play only a minor role in sustained flavin photoreduction, and in their absence, Met residues contribute to the reductive quenching process. However, even after extensive residue substitution, we fail to identify an obligatory electron donor to the excited-state flavin, thereby suggesting that without proximal Trp or Tyr residues, electron donors to the flavin are redundant. In contrast, surface Met residues have a strong influence on reduction-coupled flavin protonation. Molecular dynamics simulations indicate that solvent access to the flavin pocket is a key parameter in this process. In all, the data led to the discovery of an intriguing, nonconventional role for oxidized methionine in protonation of the reduced flavin.

MATERIALS AND METHODS

Site-Directed Mutagenesis. Tyr-less VVD-III in vector pET-28a was prepared by replacing all nine Tyr residues with Phe (Tyr:40,45,50,87,94,98,126,175,177:Phe[45]) in the context of VVD-III (Cys108Ala:Met135Ile:Met165Ile[45]) via cassette mutagenesis. Tyr-less Met-less VVD-III was generated by the Met95Leu, Met117Leu, and Met179Ile substitutions. Tyr-less Met-less VVD-II was produced by reintroducing Cys108 into the Tyr-less Met-less VVD-III construct.

Variants of LOV-HK from *Brucella abortus* in vector pET-24d (a generous gift from Drs. Rinaldi and Goldbaum) were modified by the following substitutions: Cys69Ala, Tyr59Phe, Tyr102Phe, Trp110Phe, and Ser130Gly.

Protein Expression and Purification. Tyr-less VVD-III plasmids were used to transform a CmpX13 strain modified from *E. coli* C41(DE3) with mannose permease gene *manX* exchanged for flavin transporter gene *ribM*[93] to improve flavin incorporation and protein yield. The SeMet variant was prepared by transforming auxotrophic B834 cells instead. For the Met-less and Met-less VVD-II variant, cells were also co-transformed with GROEL/ES to improve native folding and yield. Cells were grown with kanamycin and 100 mg of riboflavin per 2 L of medium in either LeMaster medium with SeMet or Miller's LB broth at 37 °C until the OD_{600} reached ∼0.8. The temperature was decreased to 17 °C, and protein expression was induced with 100 μM IPTG. After expression under constant white light illumination for 18 h, cells were pelleted at 5000*g*. Pelleted cells were either stored temporarily at −20 °C or immediately resuspended in a buffer [50 mM Hepes, 150 mM NaCl, and 10% glycerol (pH 8)] and lysed. Resuspended cells were sonicated for three cycles of 2 min (2 s on, 2 s off) until they were homogeneous, followed by centrifugation at 20000 rpm for 1 h at 4 °C. The supernatant

https://doi.org/10.1021/acs.biochem.1c00064
Biochemistry 2021, 60, 1148−1164

was loaded onto a Ni-NTA resin column, and nontagged protein contaminants were removed by washing with buffer and 20 mM imidazole. Bound protein was eluted with buffer and 200 mM imidazole, concentrated with a 10 kDa centrifugal cutoff filter, and loaded onto an equilibrated preparatory column (HiLoad 26/600 Superdex 75). Colored fractions corresponding to ∼17 kDa were collected, concentrated, aliquoted, and stored at −80 °C.

LOV-HK variants were expressed in C41(DE3) *manX*::*ribM* cells with kanamycin and 100 mg of riboflavin per 2 L of medium. Cells were grown in Miller's LB broth at 37 °C until the OD_{600} reached ∼0.8. Cultures were cooled to 25−28 °C, and protein expression was induced with 100 μM IPTG for 18 h. Cells were pelleted at 5000*g*, and proteins isolated in a manner similar to that previously described.[94] Cells were resuspended in 20 mM Tris, 0.1% Triton, 500 mM NaCl (pH 8), and 5 mM DTT and sonicated for three cycles of 2 min (2 s on, 2 s off) until homogeneous. Lysed cells were centrifuged at 20000 rpm for 1 h at 4 °C, after which, the supernatant was incubated on a Ni-NTA resin column, which was subsequently washed with DTT-free buffer and 20 mM imidazole and eluted with DTT-free buffer and 200 mM imidazole. Protein was concentrated and stored at −80 °C.

Photoreduction Rate Measurements. VVD and LOV-HK proteins were buffer-exchanged into 50 mM Hepes (pH 8), 150 mM NaCl, and 10% glycerol at least three times and adjusted to an A_{450} of 0.1−0.3 (path length of 0.2 cm, Hellma microcuvette, quartz). SEC-purified proteins that are under these conditions were used without exchanging. For GSH and H_2O_2 conditions, buffers were made fresh each time by addition of newly prepared stock reagents, and protein samples were exchanged into these buffers three times. For deuterated conditions, H_2O was substituted with D_2O and all other reagents were left unchanged. Samples were kept on ice for several hours after buffer exchanging twice or thrice to allow for enough time for deuteron exchange. Thereafter, samples were buffer exchanged once or twice more just before measurements. In a 0.2 cm quartz microcuvette, 10 μL of protein was illuminated with a 448 nm laser (30 mW, World Star; measured at 24.0 mW using a Coherent FieldMate power meter) orthogonal to the path of data collection. For lower-light intensity measurements, a ND1 filter was used to reduce the power to 2.15 mW. Kinetic traces were acquired every 0.5 s at 20 °C. Dark-state spectra were acquired for ∼5 s before laser excitation. All spectra were recorded on an Agilent 8453 diode-array spectrophotometer.

Data were processed by global analysis using Glotaran.[95] Spectra below 300 nm were removed owing to the poor signal-to-noise ratio, and data above 700 nm were discarded due to a lack of spectral features. Difference spectra were calculated by subtracting the average of the first five spectra before laser irradiation. The zero time point was defined by a fluorescence bleach at 500 nm and growth of positive spectral features. Spectra were further baseline corrected at 700 nm, and the laser line between 445 and 450 nm was set to zero to eliminate inconsistent data points.

Recovery of the Oxidized State. Samples were set up like photoreduction assays, except irradiation was halted before samples began to aggregate, as monitored at isosbestic points at 345 and 497 nm. Thereafter, samples were allowed to slowly reoxidize at 20 °C in the dark. To avoid constant irradiation from the spectrophotometer probe light, cycle times were increased to 1−10 s, depending on how rapidly recovery occurred. To confirm the probe light did not re-reduce the protein, data sets were collected at longer cycle times and compared. Traces at 455 nm were fit to a monoexponential function $\{y = a[1 - \exp(-kt)] + y_0\}$ using the curve-fitting tool in MATLAB (The MathWorks, Inc., Natick, MA) to determine the rate constants. For base-catalyzed recovery experiments, a 1 M stock of imidazole was prepared in buffer and diluted into the samples to the desired final concentration before irradiation.

Fourier Transform Infrared Difference Spectroscopy. The sample was transferred into 50 mM phosphate buffer (pH 8) and 100 mM NaCl by repeated ultrafiltration (Vivaspin 500, Sartorius, 5 kDa cutoff) at 15000*g* and 4 °C and was concentrated to an OD_{448} of ∼70. One to three microliters of the sample was placed on a BaF_2 window (Korth Kristalle) and sealed without any drying by a second window and grease. FTIR difference spectra were recorded on a Bruker IFS 66/S spectrometer equipped with a mercury cadmium telluride detector at a resolution of 2 cm^{-1} and at 20 °C. An optical filter (Spectrogon) after the sample restricted the recording range to <2000 cm^{-1} and prevented stray light on the detector; 1024 scans were recorded before and after illumination of the sample with 20 mW cm^{-2} of a 455 nm light-emitting diode (Philipps Lumileds, full width at half-maximum of 20 nm). Several experiments on independent preparations were averaged to a representative difference spectrum with a total of 3072 scans for VVD-37, 4096 scans for Tyr-less VVD-III, and 5120 scans for SeMet Tyr-less VVD-III.

Fluorescence Spectroscopy. Samples were diluted to an A_{450} of ∼0.1, as measured on an Agilent model 8453 spectrophotometer (path length of 1 cm; Hellma, micro-cuvette, quartz). Quantum yields were then measured in triplicate (path length of 5 mm; Hellma, microcell, quartz) using a Varian Cary Eclipse instrument coupled to a Quantum Northwest temperature controller at 20 °C. Excitation was set at 450 nm (bandwidth of 10 nm), and emission collected at 500 nm (bandwidth of 5 nm). Fluorescence quenching kinetic data were similarly acquired with 0−0.5 s averaging and constant stirring (path length of 1 cm; Hellma, semimicro, quartz). Rate constants were determined by a single-exponential fit using MATLAB (The MathWorks, Inc.). The quantum yield was calculated by the following:[96]

$$\Phi_i = \Phi_R \frac{F_i}{F_R} \times \frac{1 - 10^{-A_R}}{1 - 10^{-A_i}} \times \frac{{n_i}^2}{{n_R}^2}$$

where Φ_i and Φ_R are the sample and reference quantum yields, respectively, F_i and F_R are the integrated fluorescence emission intensities of the sample and the reference, respectively, A_i and A_R are the integrated excitation intensities of the sample and reference (i.e., λ_{ex} ± half-bandwidth), respectively, and n_i and n_R are the sample and reference solution indices of refraction, respectively. As buffer conditions are identical, n_i and n_R are approximated to be the same.

Circular Dichroism. SEC-purified protein samples were buffer-exchanged into 50 mM sodium phosphate (pH 8), 100 mM NaCl, and 10% glycerol. Stock concentrations were determined by a Bradford assay and subsequently diluted to ∼30 μM. Wavelength scans were collected from 200 to 260 nm at 25 °C, with 1 nm increments. Thermal melts were acquired at 220 nm from 25 to 95 °C in 2 °C increments with a 1 min equilibration time. All circular dichroism measurements were acquired using an Aviv model 202-01 CD spectrometer.

https://doi.org/10.1021/acs.biochem.1c00064
Biochemistry 2021, 60, 1148−1164

Melting temperatures were determined by fitting thermal melt traces with a logistic function using MATLAB:

$$f(x) = \frac{a}{1 + e^{b(-x+c)}} - d$$

Molar ellipticity was calculated from millidegrees as $m^{\circ} \times M/(10dC)$, where C is the concentration in milligrams per milliliter, M is the average molecular weight (grams per mole), and d is the path length of the cell (centimeters).

Electron−Nuclear Double-Resonance Spectroscopy (ENDOR) Measurements. Q-Band (~34 GHz) measurements were carried out on a Bruker E580 spectrometer equipped with a 150 W radiofrequency (RF) amplifier at 150 K. For pulse ENDOR, a Davies sequence ($\pi-\tau_1-$RF$-\tau_2-\pi/2-\tau-\pi-\tau-$echo) with a 16-step phase cycling was utilized with the π and RF pulses at 140 ns and 20 μs length, respectively. The ^{1}H Larmor frequency is ~51 MHz, and the largest hyperfine coupling for semiquinone radicals is ~30 MHz; therefore, ENDOR was measured in the range of 25−75 MHz.

Molecular Dynamics. MD simulations performed in this work were based on homology models of VVD-III obtained with Swiss Model,[97] using Protein Data Bank (PDB) entry3IS2[98] as the template, and placement of FAD afterward with SwissDock.[99] Simulations were performed in truncated octahedral boxes containing TIP4P-Ew water molecules,[100] having a buffer distance of 12 Å with the solute. Monovalent ions (Na^+ and Cl^-) were added to neutralize the boxes and provide them with ionic strengths of 150 mM. Simulations were run with a time step of 1 fs with full periodic boundary conditions. The smooth particle mesh Ewald (PME) method[101] with a 12 Å cutoff was used to calculate long-range electrostatic interactions, and the SHAKE algorithm[102] was used to constrain all bonds involving hydrogen. For constant-pressure and -temperature simulations, the Berendsen barostat[103] with a pressure relaxation time of 1 ps and isotropic pressure scaling was used along with Langevin dynamics (γ = 5.0). Before production trajectories were initiated, the MD boxes were subjected to a series of rigorous equilibration steps that are detailed elsewhere.[104] All simulations were performed with the AMBER18 software package,[105] using the pmemd.cuda program[106] and employing the Amber parm99 force field.[107] The radial distribution functions (RDFs) were calculated from the MD trajectories using the program cpptraj.[108] The RDFs were obtained considering the Cγ atom of Asn161 as the origin, using a bin size of 0.05 Å.

3D-RISM Calculations. The three-dimensional reference interaction site model (3D-RISM[109−111]) is a molecular solvation theory-based approach that has been shown to be extremely useful in predicting the solvation structure and thermodynamics of biomolecules. Here, 3D-RISM calculations were performed for all VVD variants, on randomly chosen, equally spaced MD configurations, as well as on average configurations obtained from MD simulations. Specific details underlying these calculations were chosen to be analogous to those used in an earlier work. Briefly, configurations obtained from MD simulations were stripped of all solvent molecules and ions. The one-dimensional (1D) solvent susceptibility value was separately calculated for SPC/E water[112] (55.5 M) containing 150 mM NaCl and 100 mM $MgCl_2$. The 3D-RISM calculations were then performed on the configurations using a 0.5 Å spaced 3D grid and the calculated 1D solvent susceptibility. All 1D- and 3D-RISM calculations were performed using the AMBER18 software package.[105]

RESULTS

Residues Involved in ET and PT to the VVD-III Flavin. VVD-III, which lacks the 36 N-terminal residues, adduct-forming cysteine, and the two most flavin-proximal Met residues, undergoes efficient flavin photoreduction to the neutral semiquinone.[45] To probe which residues participate in the photoreduction of VVD-III, we systematically replaced those with the least negative formal oxidation potentials, namely, Tyr, Cys, and Met [VVD-III contains no Trp or His residues (Figure 1)]. We studied the effects of these

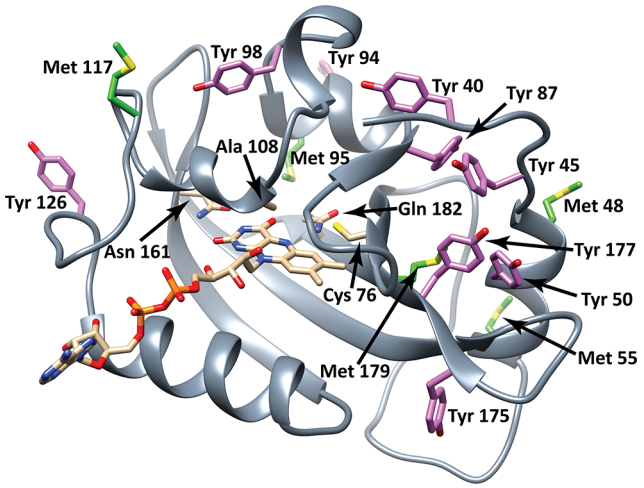

Figure 1. Homology model of VVD-III with Tyr and Met residues displayed.[97,99] Structure generated from PDB entry 3IS2[98] using Swiss Model[97] and FAD placed by SwissDock.[99]

substitutions on relative fluorescence quantum yields (FQYs) and redox-state conversion rates during constant illumination. FQYs report on the kinetics of primary ET to the excited flavin singlet S_1 state. Both flavin S_1 and triplet T_1 excited states are effective oxidants of aromatic compounds, in free solution and within proteins, with the singlet states producing faster quenching rates owing to their higher potentials and more favorable electronic coupling.[51] However, the S_1 states are much shorter lived than the T_1 states,[28,29,37,43,113] and hence, singlet-state ET quenching of flavin will be limited to proximal Trp and Tyr residues, as observed with cryptochromes and flavodoxins.[15,114] Assuming largely invariant nonradiative quenching, removal of closely localized electron donors to the flavin may be reflected by increased FQYs. In contrast, rates of ASQ and NSQ accumulation under constant illumination reflect factors that influence sustained cofactor reduction, which include recombination reactions involving multiple centers and chemical quenching of electron holes generated by electron transfer to the excited-state flavin.

Variants Generated. Initially, all nine Tyr residues were replaced with Phe to form the "Tyr-less" VVD-III variant. Cys76Val VVD-III was produced to test whether the most flavin-proximal Cys participates in photoinduced ET. In the context of both VVD-III and Tyr-less VVD-III, all Met residues were isosterically replaced with selenomethionine to create SeMet VVD-III and SeMet Tyr-less VVD-III proteins, respectively. Photoreduction kinetics were recorded in the presence of varying concentrations of oxidants (H_2O_2),

https://doi.org/10.1021/acs.biochem.1c00064
Biochemistry 2021, 60, 1148−1164

reductants [glutathione (GSH) or ascorbate], and D_2O. Note that the formal potential of SeMet (E_{pa} = 0.84 V vs NHE) is lower than that of Met (E_{pa} = 1.21 V vs NHE[115]) and SeMet is readily oxidized to the selenoxide form by peroxide (H_2O_2).[116−119] Selenoxide can in turn be reduced back to SeMet by glutathione (GSH).[120−122] Met residues are oxidized to the sulfoxide by H_2O_2,[69,123] but GSH cannot reduce methionine sulfoxide (MetSO).[120,122] In the parent Tyr-less VVD-III construct, the remaining flavin-proximal Met residues (Met95, Met117, and Met179) were substituted individually with hydrophobic (Leu or Ile) or hydrophilic (Gln) residues. Met95 and Met179 are conserved as Leu and Ile, respectively, in all phototropin LOV2 domains.[47] All three Met residues were replaced concomitantly to form the "Met-less" variant. The two remaining Met residues (48 and 55) are located on the A′α helix >20 Å from the flavin and were considered unlikely to participate in photoreduction (Supplemental Table 1). In the case of Tyr-less Met-less VVD-III, 15 of 148 VVD residues were exchanged.

In addition to VVD-III, we also investigated residue substitutions in a well-studied bacterial LOV domain from the *B. abortus* histidine kinase (LOV-HK). LOV-HK does not contain a flavin-proximal Gly residue on Iβ that is highly conserved in other LOV domains. As noted above, Gly residues can also act as electron donors to high-potential acceptors. Substitution of the analogous conserved Gly in VVD-III does not produce stable protein, whereas reintroduction of Gly into LOV-HK yields a soluble flavin-bound variant.

Fluorescence Quantum Yield Measurements. Compared to the parent VVD-III protein, replacement of all of the Tyr residues with Phe resulted in only a small FQY increase (Table 1), which indicates that nearby Tyr residues do not appreciably contribute to reductive quenching of the flavin S_1 state.[124−127] Similarly, Met and Cys substitutions have only weak effects on FQY, and thus, these residues (which have been reported to quench flavin fluorescence in aqueous solutions[128]) also are not essential for reductive quenching of the flavin S_1 state. Comparatively, analogous fluorescent LOV domain proteins (adduct Cys-less LOV-HK proteins and iLOV variants) exhibit FQYs (absolute FQY of iLOV ∼ 0.32−0.34[23]) similar to those of VVD-III and are approximately four times more fluorescent than WT adduct-forming VVD. In contrast, the *Drosophila* cryptochrome, which is functionally optimized for rapid photoreduction from a conserved Trp tetrad,[55] shows nearly no fluorescence (a very small FQY) compared to all of the LOV domain variants unless the most flavin-proximal Trp residue is substituted with a Phe residue [W420F (Table 1)]. Notably, the FQY of WT VVD is much lower than those of the Cys108Ala-derived variants (i.e., VVD-III), which implies that Cys108 promotes intersystem crossing to the T_1 state by a heavy atom effect or Cys108 can react directly with the S_1 state in VVD.

Table 1. Fluorescence Quantum Yield Ratios of VVD-III Variants[a]

Variant	Quantum yield ratio
VVD-III	≡1
VVD-III M95Q	0.94 ± 0.03
SeMet VVD-III	0.93 ± 0.03
Tyr-less VVD-III	1.06 ± 0.03
SeMet Tyr-less VVD-III	1.02 ± 0.03
Tyr-less Met-less VVD-III	1.06 ± 0.08
VVD WT	0.16 ± 0.05
VVD M95L	0.22 ± 0.03
LOV-HK C69A	1.04 ± 0.02
LOV-HK C69A:Y59F:W110F	0.94 ± 0.02
iLOV WT	0.96 ± 0.07
iLOV Q489D	0.97 ± 0.03
dCRY WT	0.00 ± 0.10
dCRY W420F	0.67 ± 0.04

[a]FQYs are calculated relative to VVD-III. The FQY of dCRY W420F reported elsewhere differs slightly owing to variabilities in protein preparation and data collection.[55]

Photoreduction Kinetics. Kinetic experiments to assess the depletion of oxidized flavin and steady-state accumulation of stable reduced states were carried out under constant illumination at 448 nm. Rates of flavin species evolution were obtained by global analysis of ultraviolet−visible (UV−vis) absorbance difference spectra and fitting all data to either two- or three-component sequential models (Figure 2). With a sequential model of increasing species lifetimes, the so-called evolution-associated spectra (EAS) represent the difference spectra relative to the ground-state oxidized flavin of the evolving species,[129] namely, fluorescence emission, ASQ, and NSQ formation (Figure 2). The variants and conditions produced three types of behavior, which are summarized in Table 2. The first case, exhibited by the VVD-III parent, VVD-III Met95Gln, and oxidized Tyr-less/SeMet proteins, displays direct NSQ formation from the fluorescent flavin, and the kinetics are well fit by a two-component sequential model with similar rate constants for these variants (Figure 3A and Table 2). Most other variants and conditions led to some accumulation of the ASQ intermediate, and their data were thus fitted with a three-component sequential model. However, these instances can be separated into two behaviors. In case 2, the EAS of the intermediate appears as a combination of the ASQ and NSQ states (Supplemental Figure 1), whereas in case 3, global analysis produces a pure difference spectrum for the ASQ (Figure 3B). Thus, in case 1, protonation rates are relatively fast compared to reduction rates and very little ASQ accumulates, whereas in case 3, protonation is slow compared to flavin reduction and an ASQ intermediate is clearly resolved. In case 2, the behavior is intermediate and a pure ASQ species is not observed under these conditions. Treating VVD-III/Tyr-less with reductant/hypoxia or substituting Cys76V/Met117/Met179 revealed some ASQ intermediate with admixtures and had similar rate constants [case 2 (Table 2 and Supplemental Figure 1C−H)]. In contrast, SeMet variants with a reducing agent, Tyr-less Met-less variants, and Tyr-less Met95Leu variants gave well-defined ASQ intermediates (Figure 3B). Generally, variants treated with oxidants have increased protonation rate constants and shift toward case 1, compared to those treated with reductants or with substituted Met

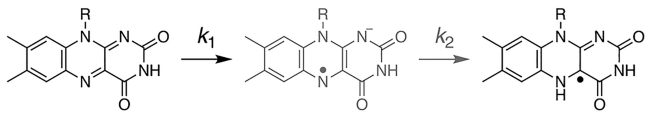

Figure 2. Sequential model for flavin photoreduction. Rate constant k_1 is attributed to the conversion of the oxidized flavin to the intermediate ASQ (gray; if observed) or directly to the NSQ species. Protonation rate constants of ASQ to NSQ are represented by k_2.

https://doi.org/10.1021/acs.biochem.1c00064
Biochemistry 2021, 60, 1148−1164

Table 2. Rate Constants of VVD-III Variants Obtained from Global Analysis[a]

Variant	k_1 [s^{-1}]
VVD-III	0.048 ± 0.013
VVD-III M95Q	0.062 ± 0.007
VVD-III M95Q + 5 mM GSH	0.087 ± 0.012
VVD-III M95Q + 5 mM H_2O_2	0.0609 ± 0.0017
SeMet VVD-III + 5 mM H_2O_2	0.040 ± 0.002
SeMet Tyr-less VVD-III + 5 mM H_2O_2	0.059 ± 0.006
Tyr-less VVD-III	0.086 ± 0.013
Tyr-less VVD-III + 5 mM H_2O_2	0.075 ± 0.006
Tyr-less C76V VVD-III + 5 mM H_2O_2	0.080 ± 0.003

Variant	k_1 [s^{-1}]	k_2 [s^{-1}]
VVD-III anaerobic	0.22 ± 0.03	0.025 ± 0.002
VVD-III + 5 mM GSH	0.28 ± 0.06	0.040 ± 0.007
Tyr-less VVD-III anaerobic	0.407 ± 0.012	0.059 ± 0.006
Tyr-less VVD-III + 5 mM GSH	0.50 ± 0.07	0.074 ± 0.007
Tyr-less VVD-III in D_2O	0.402 ± 0.010	0.0524 ± 0.0019
Tyr-less C76V VVD-III	0.568 ± 0.018	0.055 ± 0.005
Tyr-less M95L VVD-III + 5 mM H_2O_2	0.23 ± 0.06	0.031 ± 0.007
Tyr-less M117L VVD-III	0.39 ± 0.02	0.035 ± 0.002
Tyr-less M117L VVD-III + 5 mM H_2O_2	0.37 ± 0.04	0.047 ± 0.004
Tyr-less M179I VVD-III	0.29 ± 0.04	0.039 ± 0.005
Tyr-less M179I VVD-III + 5 mM H_2O_2	0.33 ± 0.06	0.040 ± 0.006

Variant	k_1 [s^{-1}]	k_2 [s^{-1}]
SeMet VVD-III + 5 mM GSH	0.181 ± 0.012	0.0226 ± 0.0008
SeMet Tyr-less VVD-III + 5 mM GSH	0.5 ± 0.2	0.034 ± 0.005
Tyr-less M95L VVD-III	0.290 ± 0.016	0.0215 ± 0.007
Tyr-less Met-less VVD-III (20% gly)	0.24 ± 0.05	0.018 ± 0.003
Tyr-less Met-less VVD-III + D_2O (20% gly)	0.207 ± 0.013	0.0173 ± 0.0010

[a]Sequential kinetics model depicted in Figure 2. Unless otherwise specified, data sets were collected in 10% (w/v) glycerol buffer for 60 s. The glycerol content was increased to 20% (w/v) for some proteins to improve stability. The left column of the table lists data sets that have no ASQ features in the EAS spectra. Data sets in the middle column exhibit ASQ intermediary species that are not fully resolved. Note that addition of 5 mM H_2O_2 to the Tyr-less single-Met variants led to a decrease in amplitude of ASQ species but did not completely eliminate the intermediate (Supplemental Figure 1). The right column contains all data sets with three well-resolved flavin EAS spectra indicative of a fully resolved ASQ intermediate.

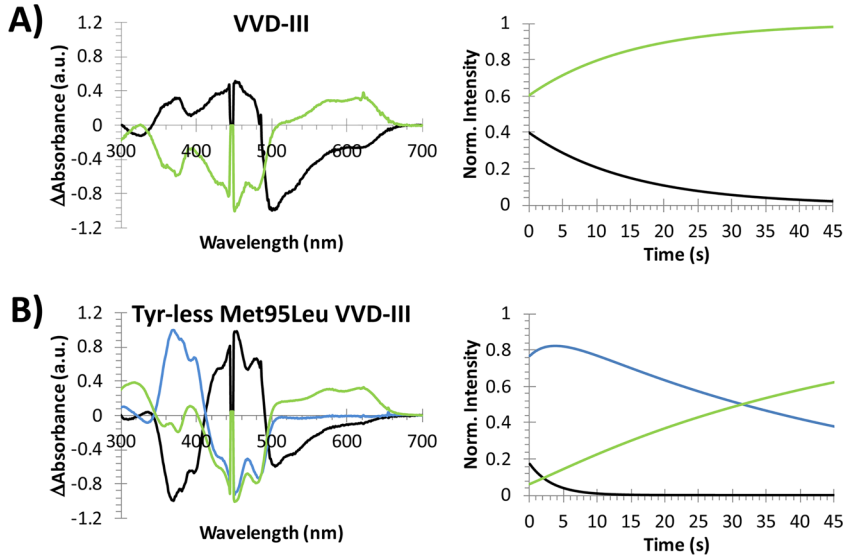

Figure 3. Representative evolution-associated spectra (EAS) and concentration profiles from global analysis of difference spectra obtained during photoreduction of VVD-III variants: (A) VVD-III and (B) Tyr-less M95L VVD-III. EAS and corresponding concentration traces are displayed in identical colors (black for ground and/or fluorescent species, blue for the ASQ intermediate, and green for the NSQ state).

residues, which generally shift toward case 3. For example, Tyr-less C76V moves from case 2 to case 1 and Tyr-less Met95Leu moves from case 3 to case 2 upon treatment with H_2O_2. In contrast, under reducing conditions, VVD-III moves from case 1 to case 2 and the SeMet variants move from case 1 to case 3. Interestingly, for those species that develop ASQ intermediates, k_1 (flavin reduction) and k_2 (flavin protonation) show a correlation that indicates similar factors affect both flavin reduction and protonation (Figure 4). This finding is a strong indication of coupling between the electron and proton transfer processes.

In terms of specific variants, Tyr-less VVD-III had a moderately increased photoreduction rate compared to that of the parent VVD-III (k_1 is ∼1.8 times greater for both untreated and reducing conditions), but at a 10-fold lower light intensity, this ratio increased [k_1 is ∼7 times greater (Supplemental Figure 2)]. These increases in photoreduction rate with the Tyr replacement may indicate that the Tyr residues facilitate charge recombination with the ASQ and thereby limit sustained photoreduction. A weaker dependence on light intensity for the faster reducing Tyr-less variants suggests that rates of sustained photoreduction begin to saturate as the radical quenching reactions become rate-limiting. VVD-III likely has a higher tolerance for increased light intensity due to internal quenching between flavin excited states and the Tyr residues. The increased accessibility of the flavin to oxygen in Tyr-less VVD-III was indicated by a faster reoxidation rate of photoreduced protein, which is 5-fold greater than that of VVD-III (Tyr-less VVD-III, 0.24 ± 0.024 min^{-1}, vs VVD-III, 0.048 ± 0.018 min^{-1}). Additional replacement of the flavin-proximal Cys76 residue [6.0 Å from flavin N5 (PDB entry 3HJI)] in conjunction with the

https://doi.org/10.1021/acs.biochem.1c00064
Biochemistry 2021, 60, 1148−1164

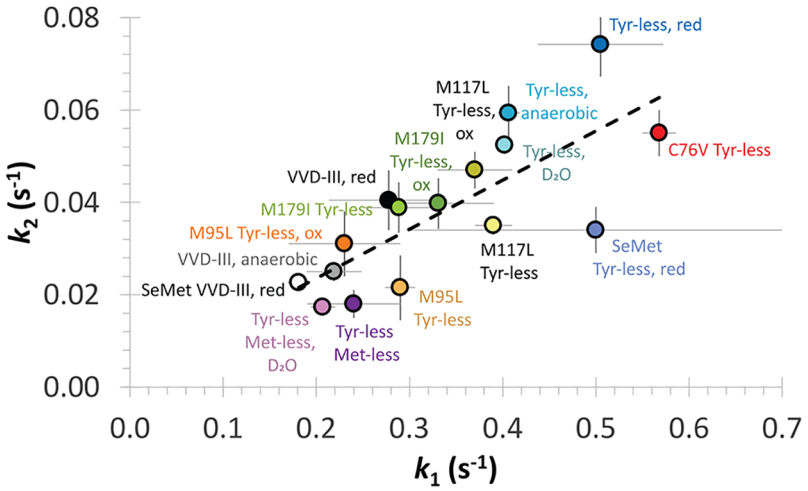

Figure 4. Correlation plot of rate constants k_1 and k_2. Data collected under oxidizing conditions are represented in darker shades. Data collected from the same variants share similar colors. The entire data set is fitted by the black linear trend line ($k_2 = 0.11k_1 + 0.002$; $R^2 = 0.6$).

removal of the native adduct-forming Cys108 (3.7 Å from flavin N5) produced a modest increase in photoreduction rate with some accumulation of ASQ. However, H_2O_2 treatment of Tyr-less C76V VVD-III, which likely affects the remaining Cys and Met residues, vanquished the ASQ intermediate. The disappearance of the ASQ implies a substantially increased protonation rate relative to the reduction rate (on the order of at least 20-fold).

To probe the role of Met residues in the photoreduction process, variants were generated either by replacement of the three most proximal Met residues (95, 117, and 179) with hydrophobic residues [Leu or Ile (Figure 1)] or by conversion of all Met residues to SeMet. Photoreduction rates were largely unaffected by SeMet substitution relative to the parent VVD-III and Tyr-less VVD-III, although the SeMet variants were especially sensitive to the reducing environment. Similar to the case for GSH-treated SeMet variants, a significant amount of ASQ species accumulated in Tyr-less Met-less VVD-III during illumination, which was further verified by Davies ENDOR (Supplemental Figure 3). The ability of remote Met residues to accelerate flavin protonation was surprising and prompted suspicions that Met substitution or modification may be altering the access of the solvent to the flavin. Solvent channel calculations using the CAVER[130] plugin in PyMOL[131] suggested that Met95 may be the primary solvent accessibility gate to the isoalloxazine binding pocket. Indeed, Tyr-less Met95Leu VVD-III exhibited the same reactivity as the Met-less variant, confirming that Met replacement at site 95 alone is sufficient to slow protonation of the ASQ. Interestingly, Met95Leu in the context of WT adduct-forming VVD has no effect on photoreduction or dark-state recovery times, even under base catalysis (Supplemental Figure 4). Other single-Met variants (Tyr-less Met117Leu VVD-III and Tyr-less Met179Ile VVD-III) behaved like the parent Tyr-less VVD-III, albeit a small amount of ASQ formed with irradiation and was not significantly decreased by peroxide treatment (Supplemental Figure 1E–H). Thus, replacement of Met with Leu or Ile stabilizes the ASQ and makes photoreduction behavior less sensitive to oxidation (with the Met95 position having the strongest effect), whereas Met replacement with SeMet sensitizes photoreduction behavior to reducing and/or oxidizing environments.

Addition of GSH to Tyr-less VVD-III and the SeMet proteins (prepared and maintained under reducing conditions with DTT) altered photoreduction rates and increased the level of accumulation of the ASQ. The differences between photoreduction rates for SeMet Tyr-less VVD-III and the Tyr-less parent treated with GSH and those for the same proteins treated with H_2O_2 were large but difficult to directly compare; in both proteins, a stable ASQ intermediate was produced with a reductant present, yet none formed under oxidizing conditions (Table 2). Hence, when Met (or SeMet) residues are the most readily oxidizable residues, a reducing environment substantially increases the rate of photoreduction, but slows flavin protonation, presumably by preventing Met oxidation. The Tyr-less Met-less and Met95Leu variants behaved like GSH-treated SeMet VVD-III samples, although their photoconversion rates were approximately half of those of the GSH-treated Tyr-less samples [both parent and SeMet variants (Table 2)]. Thus, replacement of Met95 with hydrophobic Leu removes the need for a reducing environment to slow flavin protonation. We conclude that in the absence of the Tyr residues, Met oxidation, particularly at position 95, encourages NSQ formation.

We attempted to analyze Met oxidation by bottom-up mass spectrometry; however, unfortunately the preparation of peptides caused variable extents of oxidation, and consistent results could not be obtained. The effect of oxidized Met95 (MetSO) was mimicked by substituting residue 95 with Gln, which yielded no ASQ intermediate and rate constants similar to those of VVD-III (Table 2). Furthermore, GSH had little effect on Met95Gln, thereby indicating that GSH itself does not directly provide electrons to the flavin. In contrast, ascorbate treatment increased photoreduction rates in a concentration-dependent manner indicative of collisional quenching (Supplemental Table 2). At ≥5 mM ascorbate, ASQ development could be detected in Met95Gln. Under these conditions, reduction rates were beginning to surpass proton transfer rates owing to direct quenching of the flavin by ascorbate. Nevertheless, even with high levels of ascorbate, the ASQ did not accumulate to the same levels as it did in Met95Leu.

Attempts to assess the role of proximal Gly180 in the flavin binding pocket by residue replacement led to insoluble protein. We instead turned to *B. abortus* LOV-HK, which is one of the

https://doi.org/10.1021/acs.biochem.1c00064
Biochemistry 2021, 60, 1148–1164

few LOV domains without the conserved Gly residue on Iβ, yet replacement of aromatic residues and introduction of a Gly residue into LOV-HK at the corresponding site of VVD Gly180 led to only small changes in photoreduction behavior (Supplemental Table 3). Thus, it is not likely that the conserved Gly residue participates in redox chemistry with the flavin.

Effects of Solvent Isotope Exchange and Viscosity on NSQ Formation Rates. Photoreduction of Tyr-less Met-less VVD-III in D_2O yielded a k_H/k_D of ~1.2 ± 0.3 for the photoreduction rate constant (k_1) and a k_H/k_D of ~1.04 ± 0.18 for the protonation rate constant (k_2). Solvent isotope effects for the case 1 Tyr-less variant are more difficult to assess because D_2O produces case 2 behavior. Hence, instead of comparing the globally determined rate constants, we monitored the wavelength most sensitive to ASQ formation ($\Delta Abs_{370}/Abs_{450}$) and found that deuterated buffer resulted in approximately four times more ASQ at early times than protonated buffer (Supplemental Figure 5 and Supplemental Table 4). To probe whether the modest isotope effects seen in the presence of the Met residues derived from changes in protein conformation and solvation, the effect of glycerol was investigated. Reactions run in either 10% or 20% glycerol showed nearly no difference at early time points [20–30 s (Supplemental Table 5)]. Thus, increased viscosity or stabilization effects of glycerol on NSQ conversion appear to be minimal.

Fluorescence Steady-State Quenching Measurements. The quenching of flavin fluorescence under constant illumination also monitors conversion of the oxidized flavin to a stable reduced semiquinone, albeit under different illumination conditions and lower light intensity compared to those used for absorption spectroscopy. Consistent with the absorption data at lower light intensities (Supplemental Figure 2), fluorescence quenching of Tyr-less VVD-III increases 7-fold compared to that of the parent VVD-III (Figure 5 and Table 3). Replacement of the Met residues decreases the quenching rate by more than half relative to that of Tyr-less VVD-III, with SeMet substitution giving a more modest decrease (Figure 5 and Table 3). A possible explanation for this behavior is that radicals formed on protein side chains are more effectively trapped at Met residues than at Tyr residues; thus, when Met residues harbor radicals in the absence of Tyr residues, radical recombination with the flavin slows and sustained reduction rates increase.

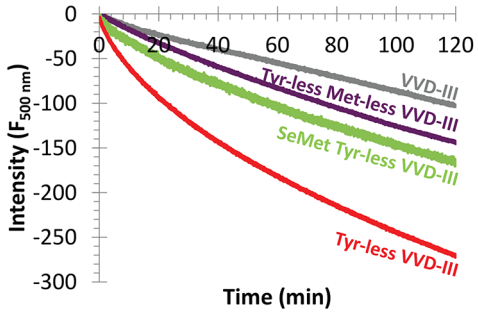

Figure 5. Steady-state fluorescence quenching of VVD-III variants with excitation at 450 nm. Each sample was acquired in pH 8 buffer without additional reductants or oxidants and using similar flavin cofactor concentrations, as measured by the integration of excitation band intensities at 450 ± 5 nm. Emission intensities were collected at 500 ± 2.5 nm. Photobleaching is largely reversible following flavin reoxidation in all variants.

Table 3. Steady-State Fluorescence Quenching Rate Constants[a]

Variant	Rate constant ($\times 10^5$ s^{-1})
VVD-III	2.61 ± 0.08
Tyr-less VVD-III	18.95 ± 0.10
SeMet Tyr-less VVD-III	12.44 ± 0.10
Tyr-less Met-less VVD-III	8.35 ± 0.06

[a]Rate constants and 95% confidence intervals obtained by fitting to a monoexponential function.

Reintroduction of the Adduct-Forming Cys Residue. Given that the residue replacements of VVD-III likely affect protein conformation, dynamics, and solvent accessibility, we evaluated whether the highly modified Tyr-less Met-less variant retains native WT functionality when the adduct-forming Cys residue[47] is returned to position 108. Reintroduction of Cys108 indeed allows for conversion to the C4a adduct species; however, the spectral properties of the variant Tyr-less Met-less VVD-II are perturbed from those of WT. Specifically, the UV–vis band is broader and blue-shifted (λ_{max} = 380 nm) (Figure 6, red trace) and, unlike that of the WT, lacks the ability to dimerize owing to the loss of Tyr40, which is an important contact in the dimer interface.[84] The broad UV–vis band resembles that of EL222 LOV[132] and implies that small structural changes in the Tyr-less Met-less VVD-II flavin binding pocket likely prevent complete photoconversion to the adduct. Nevertheless, circular dichroism measurements indicate few differences in molar ellipticity between VVD and the highly modified variant. The helical contents of Tyr-less, SeMet Tyr-less, Tyr-less Met-less, and VVD-III are similar (Supplemental Figure 6), and thermal melting occurs uniformly, with relatively small T_m differences among the variants (Supplemental Table 6).

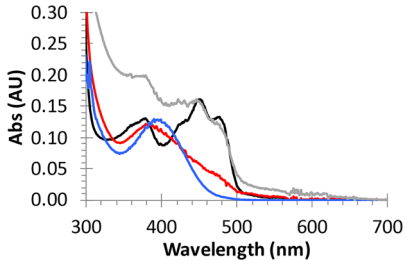

Figure 6. UV–vis spectra of Tyr-less Met-less VVD-II and WT VVD. Reintroduction of conserved Cys108 into the Tyr-less Met-less protein allows for photoreduction to the fully reduced adduct species (red) from the dark state (black). The adduct species thermally recovers (gray) to the oxidized flavin albeit with signs of aggregation. The reduced species has a λ_{max} of 380 nm, which is 10 nm blue-shifted relative to the adduct spectrum of WT VVD (blue; λ_{max} = 390 nm). VVD and the variant adduct species have three similar isosbestic points at 330, 385, and 413 nm, as previously reported for other LOV domains.[1,133,134]

Photoinduced Methionine Residue Conversion. Fourier transform infrared (FTIR) difference spectroscopy was utilized to probe changes to the VVD chemical structure after photoreduction. IR difference spectra were recorded for a given VVD protein between post- and preillumination states. To assign vibrational bands, these difference spectra were

https://doi.org/10.1021/acs.biochem.1c00064
Biochemistry 2021, 60, 1148–1164

compared first to those of a well-characterized reference protein, the aureochrome 1a LOV domain from *Phaeodactylum tricornutum* that lacked the C-terminal Jα helix (A′α-LOV).[135,136] A′α-LOV behaves like a canonical LOV domain and generates a flavin-C4a-cysteinyl adduct under blue light irradiation but lacks any structural responses from A′α or Jα. For WT VVD in the photoactivated adduct state, the flavin C_4O band shows the characteristic upshift from 1711(−) to 1725(+) cm^{-1} and the main flavin CN band shifts from 1551(−) to 1530(+) cm^{-1} (Supplemental Figure 7A). Specific to VVD, secondary structural changes at 1648(+) cm^{-1} are observed that reflect the reorganization and dimerization of α helices in the Ncap[84] accompanied by changes in turn elements at 1682(+) cm^{-1}. The deprotonation of Cys108 by adduct formation is detected at a typical frequency for a thiol vibration at 2561(−) cm^{-1} (Supplemental Figure 7B).[137]

Illumination of Tyr-less VVD-III generates a typical pattern for an NSQ with signals at 1666(+) and 1532(−) cm^{-1} from flavin CO and CN stretches (Supplemental Figure 7C).[138] Importantly, there is no signal in the thiol band region of Tyr-less VVD-III, signifying that Cys residues do not oxidize in the photoreduction of FAD to the NSQ state (Supplemental Figure 7B).

Difference spectra of Tyr-less VVD-III and SeMet Tyr-less VVD-III were compared to probe changes in Met residues during flavin photoreduction. Both difference spectra are almost identical with the prominent flavin CN bands present at 1547(−) and 1532(+) cm^{-1} in both variants upon photoconversion (Figure 7). For Tyr-less VVD-III though, there is a band at 1279(−) cm^{-1} that is not observed in the SeMet Tyr-less variant. This signal has been unambiguously identified as a Met signal for bacteriorhodopsin photoconversion at 1284(−) cm^{-1},[139] and tentatively assigned to the S−C—H bending mode of Met.[140] Hence, Met clearly participates in sustained flavin reduction in Tyr-less VVD-III and Met conversion may be related to oxidation reactions associated with radical quenching at the Met residues.

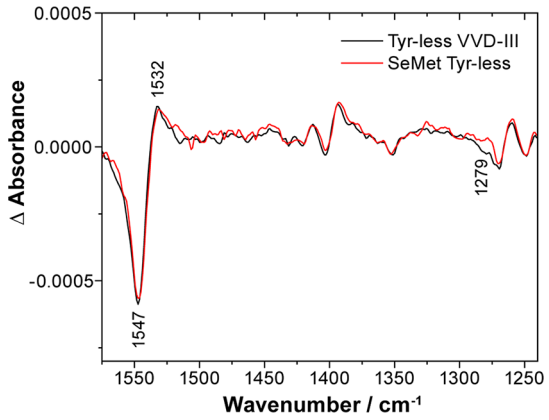

Figure 7. FTIR difference spectra of Tyr-less and SeMet Tyr-less VVD-III after illumination. Identical bands at 1547(−) and 1532(+) cm^{-1} substantiate neutral radical formation. The presence of a negative band at 1279(−) cm^{-1} only in the Tyr-less variant implicates methionine radical conversion by light.

Computational Studies of Solvent Accessibility. The kinetic data suggested that flavin protonation rates were sensitive to a range of modifications at peripheral Met residues that affected their hydrophilic nature and, presumably, their conformational dynamics. Hence, the role of Met residues, particularly Met95, in controlling the access of the solvent to the flavin binding pocket was further explored by molecular dynamics (MD) simulations. MD simulations were performed for each of the variants: VVD-III, Tyr-less, Tyr-less Met-less, Tyr-less Met95Leu, Tyr-less Met95Gln, and Met95SO (VVD-III in which Met95 was replaced with a methionine sulfoxide). Simulations were each carried out to 500 ns, and radial distribution functions (RDFs) of water molecules with the Cγ atom of Asn161 as the origin were calculated (Figure 8D). Asn161 was selected as an origin to report on the diffusion of water molecules into a polar pocket lined by Asn161, Gln182, and the flavin itself. The RDFs indicated that the Met95Gln variant allowed substantial penetration of water into this pocket owing to its increased conformational dynamics. To identify specific regions of interaction, 3D-RISM calculations[141,142] were performed to determine favorable water positions within the protein. Notably, regardless of the variant, 3D-RISM indicated that water molecules reside in the cavity vacated by the Cys108Ala substitution, albeit not to a high occupancy. However, the Met95Gln replacement increased water occupancy within the region containing Gln182 and Asn161 and, to a lesser extent, in a region near Phe159 (Figure 8A−C). Oxidation of Met95 to a sulfoxide (Met95SO) also extended the RDFs toward Asn161 (Figure 8B) but caused only minor conformational changes to residue 95, which continued to block the entryway and prevent water molecules from permeating as far into the flavin pocket as did Met95Gln (red trace in Figure 8D). Overall, the MD simulations support the assertion that increase in hydrophilicity at residue 95, through substitution or oxidation, causes heightened side-chain dynamics and increased access of water to the flavin.

DISCUSSION

Understanding the basis of VVD-III photoreduction is important for appreciating the range of mechanisms available to photoactive proteins. Moreover, VVD-III provides an opportunity to study the coupling of proton and electron transfer to the isoalloxazine ring, a process widely relevant to redox biology. In a more practical sense, such understanding is also desirable to generate photoinactive variants for circadian clock loss-of-function studies and for augmenting the fluorescence lifetimes of LOV domain reporter molecules.[13,23,25] VVD lacking the adduct-forming Cys residue still generates the active signaling state by conversion of the oxidized flavin cofactor to the neutral semiquinone.[45,92] The NSQ, like the cysteinyl adduct, has N5 protonated, which is critical for triggering the conformational changes needed for dimerization.[45,92] Usually, photoinduced ET to flavin involves redox-active relay residues, such as Trp and Tyr, as direct electron donors to the cofactor excited state.[37,125,143,144] In VVD-III, however, no Trp or Tyr residues reside within ∼10 Å of the isoalloxazine ring (Supplemental Table 1). Through residue replacement, we find that the Tyr residues play only minor roles in photoreduction, whereas Met residues may be sites of radical quenching and surprisingly affect the conversion of the anionic to the neutral semiquinone species.

The Tyr-less VVD-III variant has all Tyr residues replaced with Phe in the context of an N-terminal truncation that also removed the only native Trp residue.[134] Unlike other flavoproteins that rely on Tyr or Trp for ET,[55,144−146] the protein not only retains its photoactivity but also exhibits an increased photoreduction rate and no increase in fluorescence

https://doi.org/10.1021/acs.biochem.1c00064
Biochemistry 2021, 60, 1148−1164

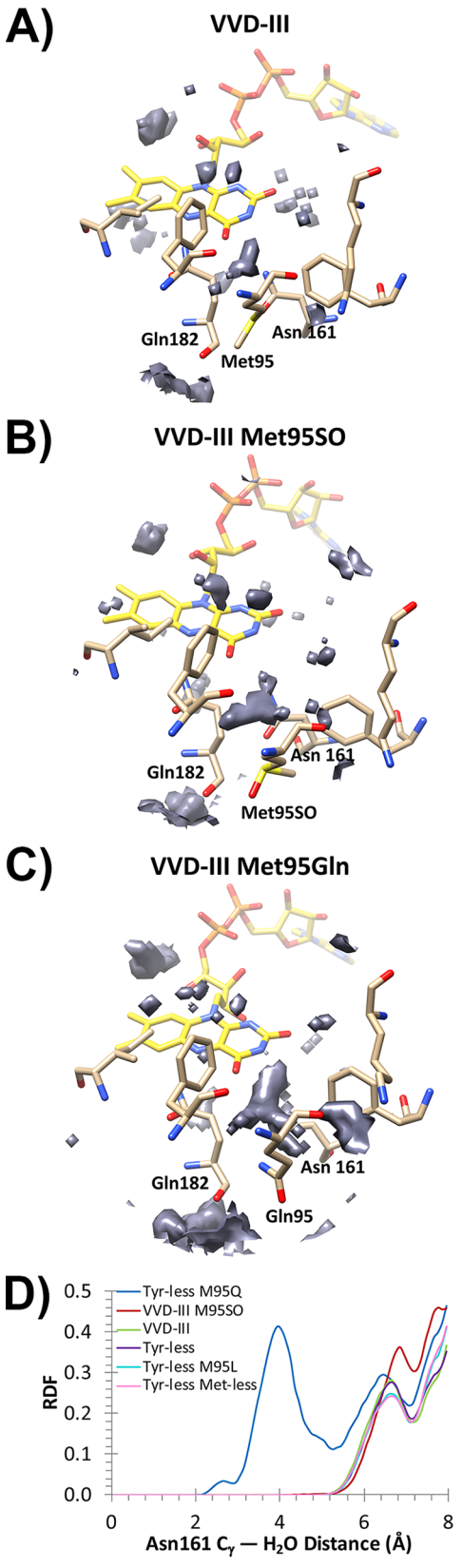

Figure 8. Molecular dynamics simulations and calculations on VVD-III homology models. (A–C) 3D-RISM calculations on VVD-III homology models to determine favorable water binding pockets at the flavin binding site. (D) Radial distribution of water molecules around the flavin binding pocket. Met95SO denotes replacement of Met95 with methionine sulfoxide.

quantum yields (Tables 1 and 2). It follows that direct ET from Tyr to the flavin excited singlet state is not a dominant mechanism for excited-state quenching in VVD. Instead, the heightened photoreduction rates upon Tyr removal may indicate the Tyr residues facilitate hole recombination with the photoreduced semiquinone and thereby slow sustained flavin reduction, which requires chemical quenching of the protein radical. Alternatively, Tyr removal could alter hydrogen-bonding networks, protein stability,[147] or the flavin environment in ways that perturb the positioning or reactivity of other electron donors to flavin. Additional substitutions of flavin-proximal Cys76 did not increase photoreduction rates over those of the Tyr-less variant, implying Cys76 is unable to sustain a thiyl radical critical for the photoreduction process. The possibility of Gly stabilizing a radical on the peptide backbone[65−67] was also ruled out by introduction of Gly at an analogous position into *Brucella* LOV-HK and the lack of an effect on photoreduction rates (Supplemental Table 3).

Global replacement of methionine residues with SeMet decreased the rate of steady-state fluorescence quenching relative to the parent Tyr-less VVD-III (Table 3), although this difference was less prominent in the parallel experiments that monitored photoreduction by UV−vis absorption spectroscopy. The discrepancy likely derives from a difference in illumination conditions, as observed in the higher relative reduction rates of Tyr-less VVD-III under lower-light intensity irradiation (Supplemental Figure 2). Thus, the Met residues may also have a role in either radical recombination or radical trapping. Free methionine is known to be a potent flavin reductant under anaerobic conditions and is capable of increasing the photoreduction rate of riboflavin in solution.[148−150] If Met residues were the primary reductive quencher of flavin in Tyr-less VVD-III, replacement with SeMet should yield faster photoreduction rates, as the oxidation potential of SeMet is considerably higher than that of Met, yet little effect was seen. Minimal effects on the FQYs upon removal of redox-active residues have implications for the involvement of the triplet state, which is the dominant reaction pathway for adduct-forming LOV domains. Intersystem crossing to T_1 precedes photoreduction despite the higher reactivity of the S_1 state, suggesting that primary donors must be a considerable distance from the flavin; this mechanism is likely similar for VVD-III variants. The inability of Met (or Tyr) substitutions to slow photoreduction also indicates that if Met (or Tyr) residues donate electrons to the flavin T_1 state, they are not the only moieties capable of doing so.

The SeMet and Tyr-less variants are, however, sensitive to the reducing environment, which in turn has a negligible effect on Met variants (Met95, Met117, and Met179 replaced by Ile or Leu in Tyr-less VVD-III). Assuming that sustained chemical quenching of proximal amino acid radical sites limits photoreduction, these ET reactions may be occurring, at least in part, at the Met residues. Consistent with this hypothesis, the FTIR data show changes in the vibrational features of Met residues after photoreduction (Figure 7). However, the photoreduction rates decrease by only approximately half when the proximal Met residues are substituted in the Tyr-less variant, which again underscores the redundancy of redox-active sites in the protein. Overall, the radical quenching mechanisms are much less efficient than initial photoinduced charge separation. Hence, the long lifetime of the high-potential flavin T_1 state allows even unfavorable and distal electron donors to act as initial electron

https://doi.org/10.1021/acs.biochem.1c00064
Biochemistry 2021, 60, 1148−1164

sources without perturbing the overall rates of ASQ accumulation.

Interestingly, oxidation of the Met and SeMet residues affects the rate of ASQ protonation. Removal of the oxide groups, which was achieved either with GSH for the SeMet variants or by substituting Met residues in the parent proteins with hydrophobic residues, greatly attenuated conversion from the ASQ to the NSQ. Therefore, in the Tyr-less VVD-III system, the Met oxidation state likely impacts the rate of flavin protonation. MD simulations indicate that the flavin protonation reactions may be related to solvent accessibility (Figure 8). Substitution of Met95 with Gln, which shows no ASQ intermediate, dramatically increases the access of the solvent to the flavin pocket by MD. Oxidation of Met95 to a sulfoxide also increases solvent penetration, but to a lesser extent, whereas the Met95Leu variant blocks solvent access. Remarkably, the single Gln substitution makes both photoreduction and NSQ formation insensitive to oxidants and reductants (Table 2 and Supplemental Table 2). The peroxide effects may also be interpreted in terms of solvent accessibility in that oxidation of the protein, which generally increases hydrophilicity, encourages greater side-chain dynamics and favors interaction with solvent. The correlation between the rate constants for flavin reduction and protonation in case 2 and case 3 variants may have a similar origin (Table 2 and Figure 4). Changes that increase solvent accessibility reveal radical sites for chemical quenching by solvent or oxygen, while also providing more facile conduits for flavin protonation.

The oxidation state of Met95, positioned at the aperture of a solvent channel that leads into the flavin binding pocket, appears to influence ASQ−NSQ conversion in VVD-III. However, Met95 is not conserved in LOV domains. The structures of homologous LOV domains commonly contain an Asn[3,151,152] in lieu of Met in the same location, which may gate water accessibility. Indeed, amide-containing side chains are known to facilitate proton movement via solvent in other LOV proteins. In the well-studied LOV2 of *Avena sativa*, Asn414 along with Gln513 coordinates water molecules to flavin for deprotonation of N5 during dark-state recovery.[3,79,153,154] Methionine sulfoxide may play a similar role in directing water molecules into the flavin pocket. The stabilization of ASQ by Met95Leu emphasizes the influence of a surface redox-inactive hydrophobic residue on solvent penetration. Other single-Met variants such as Tyr-less Met117Leu and Tyr-less Met179Ile also facilitate buildup of the ASQ and are largely insensitive to oxidants, suggesting smaller but significant roles for oxidized Met117 and Met179 in flavin protonation (Supplemental Figure 5 and Supplemental Table 4). To further probe the role of solvation in photoreduction, solvent isotope effects on VVD-III photoreduction and flavin protonation were probed by solvent exchange into D_2O. The Tyr-less Met-less variant gave nearly no isotope effect (k_H/k_D) for both k_1 and k_2, whereas Tyr-less alone produced significantly more ASQ in D_2O. These changes are likely partly the result of perturbed solvation on protein conformation and dynamics but could also reflect the role Met residues play in both sustained reduction and facilitating flavin protonation.

The overall integrity of the Tyr-less Met-less VVD-III construct and its flavin binding pocket was substantiated via the reintroduction of conserved Cys108, which resulted in the fully reduced adduct state upon irradiation with blue light (Figure 6). Thus, large scale changes to redox-active residues in VVD do not appreciably alter the ability to form the adduct state or recover to the dark state. This strictly conserved Cys in LOV domain systems has been identified as the primary proton donor to N5 of the isoalloxazine ring[28,35,43,79] and forms a neutral radical pair intermediate with flavin (NSQ−Cys$^{\bullet}$) before radical recombination to generate the adduct species, although the specifics are still debated.[31,32,155] Cys108 clearly increases the N5 protonation rate by providing a neighboring proton source and facilitating concerted direct electron donation.[37,38] The increase in the FQY upon the Cys108Ala substitution suggests that the S_1 state may participate directly in adduct formation. Whereas LOV proteins are known to primarily form cysteinyl adducts from the T_1 state,[28,29,37,43,113] substantial S_1 reactivity has been observed in some cases[156] and predicted computationally in others.[33] Alternatively, spin−orbit coupling between the flavin and the cysteine sulfur could increase the intersystem crossing rate.[157,158]

Met residues exhibit various structural and electronic functions in proteins, and oxidation of internal Met residues often leads to thermal destabilization, misfolding, and degradation.[159,160] In amyloid β peptides, Met oxidation can disrupt the local internal environment, causing expanded conformations, aggregation, and ultimately disease states in Alzheimer's and Parkinson's disease.[159,161] Additionally, photooxidation of ribonuclease A causes a 67% loss of native activity, which has been attributed to conformational changes by the oxidized Met residues.[162] Surface Met residues, on the contrary, exhibit protective roles as ROS sinks,[163−166] and Met oxidation can serve to buffer against oxidative damage to proteins, as in the case of bovine growth hormone[167,168] and glutamine synthetase.[71] Met residues in VVD do not have an obvious structural role, although flavin-proximal Met residues have been demonstrated to tune dark-state recovery rates, likely owing to an effect on flavin electronics.[98] Interactions between reduced Met and aromatic residues are widely found as structural stabilizing motifs,[169−171] yet Met oxidation in VVD does not cause structural instability. Our studies of Tyr-less VVD-III instead reveal a substantial impact of Met on light-driven redox reactions.

CONCLUSION

VVD-III and its variants readily form the signal-competent NSQ species under blue light irradiation regardless of the availability of typical redox-active residues, specifically Tyr, Cys, and Met. That said, VVD-III photoreduction is not nearly as efficient as that of cryptochrome proteins. Unlike the dedicated Trp tetrad in cryptochromes, electron sources for the excited-state VVD-III flavin are redundant, with large scale substitutions of Tyr, Met, Gly, and Cys residues having only modest effects on sustained photoreduction rates. Tyr residues likely do play a role as intermediate reductive quenchers but also facilitate recombination of the charge-separated species to limit hole propagation and sustained photoreduction. Stable reduction of the protein under constant illumination requires the system to escape these recombination reactions. Met residues contribute to reductive quenching but also serve as secondary relay residues and sites of radical quenching. The redox environment affects Met oxidation states, which in turn influence radical quenching, access of the solvent to the flavin pocket, and flavin PCET. Peripheral Met residues, primarily Met95, facilitate proton transfer to the ASQ in their oxidized states, much like conserved polar residues found at these locations in other LOV proteins. Small alterations in peripheral

https://doi.org/10.1021/acs.biochem.1c00064
Biochemistry 2021, 60, 1148−1164

residues gate NSQ conversion by altering the access of the solvent to the flavin pocket. Overall, these findings emphasize the utility of the flavin cofactor as a photosensitizer for the evolution of photosensory proteins. The high potential of the flavin excited states (>2.0 eV) allows for a considerable degree of tolerance for effective electron-donating groups, and thus, the reactivity of excited-state flavins has great potential for driving chemistry yet also presents challenges for precise control.

■ ASSOCIATED CONTENT

Supporting Information

The Supporting Information is available free of charge at https://pubs.acs.org/doi/10.1021/acs.biochem.1c00064.

Supplemental figures, including evolution-associated spectra, Davies ENDOR, photoreduction and recovery traces, circular dichroism, and FTIR difference spectra, and supplemental tables of photoreduction rate constants and global fits, circular dichroism thermal melt fits, and quantification of maximum ASQ formation (PDF)

Accession Codes

VVD, Q9C3Y6; LOV-HK, Q8YC53.

■ AUTHOR INFORMATION

Corresponding Author

Brian R. Crane − *Department of Chemistry and Chemical Biology, Cornell University, Ithaca, New York 14853, United States;* orcid.org/0000-0001-8234-9991; Phone: (607) 254-8634; Email: bc69@cornell.edu

Authors

Estella F. Yee − *Department of Chemistry and Chemical Biology, Cornell University, Ithaca, New York 14853, United States;* orcid.org/0000-0001-7108-1387

Sabine Oldemeyer − *Physical and Biophysical Chemistry, Department of Chemistry, Bielefeld University, 33615 Bielefeld, Germany*

Elena Böhm − *Physical and Biophysical Chemistry, Department of Chemistry, Bielefeld University, 33615 Bielefeld, Germany*

Abir Ganguly − *Laboratory for Biomolecular Simulation Research and Institute for Quantitative Biomedicine, Rutgers, The State University of New Jersey, Piscataway, New Jersey 08854-8076, United States*

Darrin M. York − *Laboratory for Biomolecular Simulation Research, Institute for Quantitative Biomedicine, and Department of Chemistry and Chemical Biology, Rutgers, The State University of New Jersey, Piscataway, New Jersey 08854-8076, United States;* orcid.org/0000-0002-9193-7055

Tilman Kottke − *Physical and Biophysical Chemistry, Department of Chemistry, Bielefeld University, 33615 Bielefeld, Germany;* orcid.org/0000-0001-8080-9579

Complete contact information is available at: https://pubs.acs.org/10.1021/acs.biochem.1c00064

Funding

This work was financially supported by National Science Foundation (NSF) Grant MCB1715233 (to B.R.C.) and DFG Grant KO3580/1-2 (to T.K.). A.G. and D.M.Y. are grateful for the financial support provided by the National Institutes of Health (Grant GM62248 to D.M.Y.). Computational resources were provided by the National Institutes of Health under Grant S10OD012346, the Office of Advanced Research Computing (OARC) at Rutgers, the State University of New Jersey, Rutgers Discovery Information Institute (RDI2), the State University of New Jersey, and the Extreme Science and Engineering Discovery Environment (XSEDE), specifically resources COMET and COMET GPU, which is supported by NSF Grant ACI-1548562 (Allocation TG-CHE190067).[172] A.G. and D.M.Y. also acknowledge the Texas Advanced Computing Center (TACC) at The University of Texas at Austin for providing HPC resources that have contributed to the research results reported within this paper.

Notes

The authors declare no competing financial interest.

■ ACKNOWLEDGMENTS

The authors are grateful to Joanne Widom for helping to generate the DNA constructs of Tyr-less VVD-III and Tyr-less VVD-III C76V and to Siddarth Chandrasekaran for collecting Davies ENDOR spectra. The authors thank Jimena Rinaldi (Estructural-Fundación Instituto Leloir, Patricias Argentinas) for the clone to express *B. abortus* LOV-HK.

■ REFERENCES

(1) Salomon, M., Christie, J. M., Knieb, E., Lempert, U., and Briggs, W. R. (2000) Photochemical and Mutational Analysis of the FMN-Binding Domains of the Plant Blue Light Receptor, Phototropin. *Biochemistry 39* (31), 9401−9410.

(2) Christie, J. M., Salomon, M., Nozue, K., Wada, M., and Briggs, W. R. (1999) LOV (Light, Oxygen, or Voltage) Domains of the Blue-Light Photoreceptor Phototropin (Nph1): Binding Sites for the Chromophore Flavin Mononucleotide. *Proc. Natl. Acad. Sci. U. S. A. 96* (15), 8779−8783.

(3) Halavaty, A. S., and Moffat, K. (2007) N- and C-Terminal Flanking Regions Modulate Light-Induced Signal Transduction in the LOV2 Domain of the Blue Light Sensor Phototropin 1 from Avena Sativa. *Biochemistry 46* (49), 14001−14009.

(4) Briggs, W. R., and Huala, E. (1999) Blue-Light Photoreceptors in Higher Plants. *Annu. Rev. Cell Dev. Biol. 15*, 33−62.

(5) Gaidenko, T. A., Kim, T. J., Weigel, A. L., Brody, M. S., and Price, C. W. (2006) The Blue-Light Receptor YtvA Acts in the Environmental Stress Signaling Pathway of Bacillus Subtilis. *J. Bacteriol. 188* (17), 6387−6395.

(6) Möglich, A., and Moffat, K. (2007) Structural Basis for Light-Dependent Signaling in the Dimeric LOV Domain of the Photosensor YtvA. *J. Mol. Biol. 373* (1), 112−126.

(7) Sancar, A. (2003) Structure and Function of DNA Photolyase. *Chem. Rev. 103*, 2203−2237.

(8) Weber, S. (2005) Light-Driven Enzymatic Catalysis of DNA Repair: A Review of Recent Biophysical Studies on Photolyase. *Biochim. Biophys. Acta, Bioenerg. 1707* (1), 1−23.

(9) Armitage, J. P., and Hellingwerf, K. J. (2003) Light-Induced Behavioral Responses ('phototaxis') in Prokaryotes. *Photosynth. Res. 76* (1−3), 145−155.

(10) Masuda, S., and Ono, T. A. (2004) Biochemical Characterization of the Major Adenylyl Cyclase, Cya1, in the Cyanobacterium Synechocystis Sp. PCC 6803. *FEBS Lett. 577* (1−2), 255−258.

(11) Sancar, A. (2000) Cryptochrome: The Second Photoactive Pigment in the Eye and Its Role in Circadian Photoreception. *Annu. Rev. Biochem. 69* (1), 31−67.

(12) van der Horst, G. T. J., Muijtjens, M., Kobayashi, K., Takano, R., Kanno, S. I., Takao, M., de Wit, J., Verkerk, A., Eker, A. P. M., van Leenen, D., Buijs, R., Bootsma, D., Hoeijmakers, J. H. J., and Yasui, A. (1999) Mammalian Cry1 and Cry2 Are Essential for Maintenance of Circadian Rhythms. *Nature 398* (6728), 627−630.

(13) Conrad, K. S., Manahan, C. C., and Crane, B. R. (2014) Photochemistry of Flavoprotein Light Sensors. *Nat. Chem. Biol. 10* (10), 801−809.
(14) Zoltowski, B. D., and Gardner, K. H. (2011) Tripping the Light Fantastic: Blue-Light Photoreceptors as Examples of Environmentally Modulated Protein-Protein Interactions. *Biochemistry 50* (1), 4−16.
(15) Kao, Y.-T., Saxena, C., He, T.-F., Guo, Li., Wang, L., Sancar, A., and Zhong, D. (2008) Ultrafast Dynamics of Flavins in Five Redox States. *J. Am. Chem. Soc. 130* (39), 13132−13139.
(16) Liu, B., Liu, H., Zhong, D., and Lin, C. (2010) Searching for a Photocycle of the Cryptochrome Photoreceptors. *Curr. Opin. Plant Biol. 13* (5), 578−586.
(17) Holzer, W., Penzkofer, A., and Hegemann, P. (2005) Photophysical and Photochemical Excitation and Relaxation Dynamics of LOV Domains of Phot from Chlamydomonas reinhardtii. *J. Lumin. 112* (1), 444−448.
(18) Ganguly, A., Manahan, C. C., Top, D., Yee, E. F., Lin, C., Young, M. W., Thiel, W., and Crane, B. R. (2016) Changes in Active Site Histidine Hydrogen Bonding Trigger Cryptochrome Activation. *Proc. Natl. Acad. Sci. U. S. A. 113* (36), 10073−10078.
(19) Vaidya, A. T., Top, D., Manahan, C. C., Tokuda, J. M., Zhang, S., Pollack, L., Young, M. W., and Crane, B. R. (2013) Flavin Reduction Activates Drosophila Cryptochrome. *Proc. Natl. Acad. Sci. U. S. A. 110* (51), 20455−20460.
(20) Ganguly, A., Thiel, W., and Crane, B. R. (2017) Glutamine Amide Flip Elicits Long Distance Allosteric Responses in the LOV Protein Vivid. *J. Am. Chem. Soc. 139* (8), 2972−2980.
(21) Anderson, S., Dragnea, V., Masuda, S., Ybe, J., Moffat, K., and Bauer, C. (2005) Structure of a Novel Photoreceptor, the BLUF Domain of AppA from Rhodobacter sphaeroides. *Biochemistry 44* (22), 7998−8005.
(22) Kennis, J. T. M., and Mathes, T. (2013) Molecular Eyes: Proteins That Transform Light into Biological Information. *Interface Focus 3* (5), 20130005.
(23) Losi, A., Gardner, K. H., and Möglich, A. (2018) Blue-Light Receptors for Optogenetics. *Chem. Rev. 118* (21), 10659−10709.
(24) Herrou, J., and Crosson, S. (2011) Function, Structure and Mechanism of Bacterial Photosensory LOV Proteins. *Nat. Rev. Microbiol. 9* (10), 713−723.
(25) Pudasaini, A., El-Arab, K. K., and Zoltowski, B. D. (2015) LOV-Based Optogenetic Devices: Light-Driven Modules to Impart Photoregulated Control of Cellular Signaling. *Front. Mol. Biosci. 2*, 18.
(26) Fujisawa, T., and Masuda, S. (2018) Light-Induced Chromophore and Protein Responses and Mechanical Signal Transduction of BLUF Proteins. *Biophys. Rev. 10* (2), 327−337.
(27) Seifert, S., and Brakmann, S. (2018) LOV Domains in the Design of Photoresponsive Enzymes. *ACS Chem. Biol. 13* (8), 1914−1920.
(28) Kennis, J. T. M., Crosson, S., Gauden, M., Van Stokkum, I. H. M., Moffat, K., and Van Grondelle, R. (2003) Primary Reactions of the LOV2 Domain of Phototropin, a Plant Blue-Light Photoreceptor. *Biochemistry 42* (12), 3385−3392.
(29) Swartz, T. E., Corchnoy, S. B., Christie, J. M., Lewis, J. W., Szundi, I., Briggs, W. R., and Bogomolni, R. A. (2001) The Photocycle of a Flavin-Binding Domain of the Blue Light Photoreceptor Phototropin. *J. Biol. Chem. 276* (39), 36493−36500.
(30) Alexandre, M. T. A., Domratcheva, T., Bonetti, C., Van Wilderen, L. J. G. W., Van Grondelle, R., Groot, M. L., Hellingwerf, K. J., and Kennis, J. T. M. (2009) Primary Reactions of the LOV2 Domain of Phototropin Studied with Ultrafast Mid-Infrared Spectroscopy and Quantum Chemistry. *Biophys. J. 97* (1), 227−237.
(31) Pfeifer, A., Majerus, T., Zikihara, K., Matsuoka, D., Tokutomi, S., Heberle, J., and Kottke, T. (2009) Time-Resolved Fourier Transform Infrared Study on Photoadduct Formation and Secondary Structural Changes within the Phototropin LOV Domain. *Biophys. J. 96* (4), 1462−1470.
(32) Bauer, C., Rabl, C. R., Heberle, J., and Kottke, T. (2011) Indication for a Radical Intermediate Preceding the Signaling State in the LOV Domain Photocycle. *Photochem. Photobiol. 87* (3), 548−553.
(33) Nakagawa, S., Weingart, O., and Marian, C. M. (2017) Dual Photochemical Reaction Pathway in Flavin-Based Photoreceptor LOV Domain: A Combined Quantum-Mechanics/Molecular-Mechanics Investigation. *J. Phys. Chem. B 121* (41), 9583−9596.
(34) Dittrich, M., Freddolino, P. L., and Schulten, K. (2005) When Light Falls in LOV: A Quantum Mechanical/Molecular Mechanical Study of Photoexcitation in Phot-LOV1 of Chlamydomonas reinhardtii. *J. Phys. Chem. B 109* (26), 13006−13013.
(35) Neiß, C., and Saalfrank, P. (2003) Ab Initio Quantum Chemical Investigation of the First Steps of the Photocycle of Phototropin: A Model Study. *Photochem. Photobiol. 77* (1), 101.
(36) Chang, X. P., Gao, Y. J., Fang, W. H., Cui, G., and Thiel, W. (2017) Quantum Mechanics/Molecular Mechanics Study on the Photoreactions of Dark- and Light-Adapted States of a Blue-Light YtvA LOV Photoreceptor. *Angew. Chem., Int. Ed. 56* (32), 9341−9345.
(37) Kutta, R. J., Magerl, K., Kensy, U., and Dick, B. (2015) A Search for Radical Intermediates in the Photocycle of LOV Domains. *Photochem. Photobiol. Sci. 14* (2), 288−299.
(38) Domratcheva, T., Fedorov, R., and Schlichting, I. (2006) Analysis of the Primary Photocycle Reactions Occurring in the Light, Oxygen, and Voltage Blue-Light Receptor by Multiconfigurational Quantum-Chemical Methods. *J. Chem. Theory Comput. 2* (6), 1565−1574.
(39) Kay, C. W. M., Schleicher, E., Kuppig, A., Hofner, H., Rüdiger, W., Schleicher, M., Fischer, M., Bacher, A., Weber, S., and Richter, G. (2003) Blue Light Perception in Plants: Detection and Characterization of a Light-Induced Neutral Flavin Radical in a C450A Mutant of Phototropin. *J. Biol. Chem. 278* (13), 10973−10982.
(40) Lanzl, K., Nöll, G., and Dick, B. (2008) LOV1 Protein from Chlamydomonas reinhardtii Is a Template for the Photoadduct Formation of FMN and Methylmercaptane. *ChemBioChem 9* (6), 861−864.
(41) Lanzl, K., Sanden-Flohe, M. V., Kutta, R. J., and Dick, B. (2010) Photoreaction of Mutated LOV Photoreceptor Domains from Chlamydomonas reinhardtii with Aliphatic Mercaptans: Implications for the Mechanism of Wild Type LOV. *Phys. Chem. Chem. Phys. 12* (25), 6594−6604.
(42) Richter, G., Weber, S., Römisch, W., Bacher, A., Fischer, M., and Eisenreich, W. (2005) Photochemically Induced Dynamic Nuclear Polarization in a C450A Mutant of the LOV2 Domain of the Avena sativa Blue-Light Receptor Phototropin. *J. Am. Chem. Soc. 127* (49), 17245−17252.
(43) Kottke, T., Heberle, J., Hehn, D., Dick, B., and Hegemann, P. (2003) Phot-LOV1: Photocycle of a Blue-Light Receptor Domain from the Green Alga Chlamydomonas reinhardtii. *Biophys. J. 84* (2), 1192−1201.
(44) Nöll, G., Hauska, G., Hegemann, P., Lanzl, K., Nöll, T., von Sanden-Flohe, M., and Dick, B. (2007) Redox Properties of LOV Domains: Chemical versus Photochemical Reduction, and Influence on the Photocycle. *ChemBioChem 8* (18), 2256−2264.
(45) Yee, E. F., Diensthuber, R. P., Vaidya, A. T., Borbat, P. P., Engelhard, C., Freed, J. H., Bittl, R., Möglich, A., and Crane, B. R. (2015) Signal Transduction in Light-Oxygen-Voltage Receptors Lacking the Adduct-Forming Cysteine Residue. *Nat. Commun. 6* (1), 10079.
(46) Tsukuno, H., Ozeki, K., Kobayashi, I., Hisatomi, O., and Mino, H. (2018) Flavin-Radical Formation in the Light-Oxygen-Voltage-Sensing Domain of the Photozipper Blue-Light Sensor Protein. *J. Phys. Chem. B 122* (38), 8819−8823.
(47) Crosson, S., and Moffat, K. (2001) Structure of a Flavin-Binding Plant Photoreceptor Domain: Insights into Light-Mediated Signal Transduction. *Proc. Natl. Acad. Sci. U. S. A. 98* (6), 2995−3000.
(48) Sato, Y., Iwata, T., Tokutomi, S., and Kandori, H. (2005) Reactive Cysteine Is Protonated in the Triplet Excited State of the LOV2 Domain in Adiantum Phytochrome3. *J. Am. Chem. Soc. 127* (4), 1088−1089.

https://doi.org/10.1021/acs.biochem.1c00064
Biochemistry 2021, 60, 1148−1164

(49) Migliore, A., Polizzi, N. F., Therien, M. J., and Beratan, D. N. (2014) Biochemistry and Theory of Proton-Coupled Electron Transfer. *Chem. Rev. 114* (7), 3381−3465.
(50) Heelis, P. F., Okamura, T., and Sancar, A. (1990) Excited-State Properties of Escherichia coli DNA Photolyase in the Picosecond to Millisecond Time Scale. *Biochemistry 29* (24), 5694−5698.
(51) Porcal, G., Bertolotti, S. G., Previtali, C. M., and Encinas, M. V. (2003) Electron Transfer Quenching of Singlet and Triplet Excited States of Flavins and Lumichrome by Aromatic and Aliphatic Electron Donors. *Phys. Chem. Chem. Phys. 5* (19), 4123.
(52) Harriman, A. (1987) Further Comments on the Redox Potentials of Tryptophan and Tyrosine. *J. Phys. Chem. 91* (24), 6102−6104.
(53) Ishikita, H., and Knapp, E. W. (2006) Function of Redox-Active Tyrosine in Photosystem II. *Biophys. J. 90* (11), 3886−3896.
(54) Nag, L., Sournia, P., Myllykallio, H., Liebl, U., and Vos, M. H. (2017) Identification of the $TyrOH^{\bullet+}$ Radical Cation in the Flavoenzyme TrmFO. *J. Am. Chem. Soc. 139* (33), 11500−11505.
(55) Lin, C., Top, D., Manahan, C. C., Young, M. W., and Crane, B. R. (2018) Circadian Clock Activity of Cryptochrome Relies on Tryptophan-Mediated Photoreduction. *Proc. Natl. Acad. Sci. U. S. A. 115* (15), 3822−3827.
(56) Liu, Z., Tan, C., Guo, X., Li, J., Wang, L., Sancar, A., and Zhong, D. (2013) Determining Complete Electron Flow in the Cofactor Photoreduction of Oxidized Photolyase. *Proc. Natl. Acad. Sci. U. S. A. 110* (32), 12966−12971.
(57) Nag, L., Lukacs, A., and Vos, M. H. (2019) Short-Lived Radical Intermediates in the Photochemistry of Glucose Oxidase. *ChemPhysChem 20* (14), 1793−1798.
(58) Zhong, D., and Zewail, A. H. (2001) Femtosecond Dynamics of Flavoproteins: Charge Separation and Recombination in Riboflavine (Vitamin B2)-Binding Protein and in Glucose Oxidase Enzyme. *Proc. Natl. Acad. Sci. U. S. A. 98* (21), 11867−11872.
(59) Wang, M., Gao, J., Müller, P., and Giese, B. (2009) Electron Transfer in Peptides with Cysteine and Methionine as Relay Amino Acids. *Angew. Chem., Int. Ed. 48* (23), 4232−4234.
(60) Glass, R. S., Schöneich, C., Wilson, G. S., Nauser, T., Yamamoto, T., Lorance, E., Nichol, G. S., and Ammam, M. (2011) Neighboring Pyrrolidine Amide Participation in Thioether Oxidation. Methionine as a "Hopping" Site. *Org. Lett. 13* (11), 2837−2839.
(61) Cordes, M., and Giese, B. (2009) Electron Transfer in Peptides and Proteins. *Chem. Soc. Rev. 38*, 892−901.
(62) Giese, B., Wang, M., Gao, J., Stoltz, M., Müller, P., and Graber, M. (2009) Electron Relay Race in Peptides. *J. Org. Chem. 74* (10), 3621−3625.
(63) Monney, N. P. A., Bally, T., and Giese, B. (2015) Proline as a Charge Stabilizing Amino Acid in Peptide Radical Cations. *J. Phys. Org. Chem. 28* (5), 347−353.
(64) Nathanael, J. G., Gamon, L. F., Cordes, M., Rablen, P. R., Bally, T., Fromm, K. M., Giese, B., and Wille, U. (2018) Amide Neighbouring-Group Effects in Peptides: Phenylalanine as Relay Amino Acid in Long-Distance Electron Transfer. *ChemBioChem 19* (9), 922−926.
(65) Shisler, K. A., and Broderick, J. B. (2014) Glycyl Radical Activating Enzymes: Structure, Mechanism, and Substrate Interactions. *Arch. Biochem. Biophys. 546*, 64−71.
(66) Backman, L. R. F., Funk, M. A., Dawson, C. D., and Drennan, C. L. (2017) New Tricks for the Glycyl Radical Enzyme Family. *Crit. Rev. Biochem. Mol. Biol. 52* (6), 674−695.
(67) Marquet, A., Tse Sum Bui, B., Smith, A. G., and Warren, M. J. (2007) Iron-Sulfur Proteins as Initiators of Radical Chemistry. *Nat. Prod. Rep. 24* (5), 1027−1040.
(68) Stubbe, J., and van der Donk, W. A. (1998) Protein Radicals in Enzyme Catalysis. *Chem. Rev. 98* (2), 705−762.
(69) Vogt, W. (1995) Oxidation of Methionyl Residues in Proteins: Tools, Targets, and Reversal. *Free Radical Biol. Med. 18* (1), 93−105.
(70) Levine, R. L., Mosoni, L., Berlett, B. S., and Stadtman, E. R. (1996) Methionine Residues as Endogenous Antioxidants in Proteins. *Proc. Natl. Acad. Sci. U. S. A. 93* (26), 15036−15040.
(71) Kim, G., Weiss, S. J., and Levine, R. L. (2014) Methionine Oxidation and Reduction in Proteins. *Biochim. Biophys. Acta, Gen. Subj. 1840*, 901−905.
(72) Teo, R. D., Wang, R., Smithwick, E. R., Migliore, A., Therien, M. J., and Beratan, D. N. (2019) Mapping Hole Hopping Escape Routes in Proteins. *Proc. Natl. Acad. Sci. U. S. A. 116* (32), 15811−15816.
(73) Hense, A., Herman, E., Oldemeyer, S., and Kottke, T. (2015) Proton Transfer to Flavin Stabilizes the Signaling State of the Blue Light Receptor Plant Cryptochrome. *J. Biol. Chem. 290* (3), 1743−1751.
(74) Kottke, T., Batschauer, A., Ahmad, M., and Heberle, J. (2006) Blue-Light-Induced Changes in Arabidopsis Cryptochrome 1 Probed by FTIR Difference Spectroscopy. *Biochemistry 45* (8), 2472−2479.
(75) Damiani, M. J., Nostedt, J. J., and O'Neill, M. A. (2011) Impact of the N5-Proximal Asn on the Thermodynamic and Kinetic Stability of the Semiquinone Radical in Photolyase. *J. Biol. Chem. 286* (6), 4382−4391.
(76) Song, S. H., Freddolino, P. L., Nash, A. I., Carroll, E. C., Schulten, K., Gardner, K. H., and Larsen, D. S. (2011) Modulating LOV Domain Photodynamics with a Residue Alteration Outside the Chromophore Binding Site. *Biochemistry 50* (13), 2411−2423.
(77) Chan, R. H., and Bogomolni, R. A. (2012) Structural Water Cluster as a Possible Proton Acceptor in the Adduct Decay Reaction of Oat Phototropin 1 LOV2 Domain. *J. Phys. Chem. B 116* (35), 10609−10616.
(78) Freddolino, P. L., Gardner, K. H., and Schulten, K. (2013) Signaling Mechanisms of LOV Domains: New Insights from Molecular Dynamics Studies. *Photochem. Photobiol. Sci. 12*, 1158−1170.
(79) Zayner, J. P., and Sosnick, T. R. (2014) Factors That Control the Chemistry of the LOV Domain Photocycle. *PLoS One 9* (1), No. e87074.
(80) Lokhandwala, J., Silverman Y De La Vega, R. I., Hopkins, H. C., Britton, C. W., Rodriguez-Iglesias, A., Bogomolni, R., Schmoll, M., and Zoltowski, B. D. (2016) A Native Threonine Coordinates Ordered Water to Tune Light-Oxygen-Voltage (LOV) Domain Photocycle Kinetics and Osmotic Stress Signaling in Trichoderma reesei ENVOY. *J. Biol. Chem. 291* (28), 14839−14850.
(81) Müller, P., Brettel, K., Grama, L., Nyitrai, M., and Lukacs, A. (2016) Photochemistry of Wild-Type and N378D Mutant E. coli DNA Photolyase with Oxidized FAD Cofactor Studied by Transient Absorption Spectroscopy. *ChemPhysChem 17* (9), 1329−1340.
(82) Paulus, B., Bajzath, C., Melin, F., Heidinger, L., Kromm, V., Herkersdorf, C., Benz, U., Mann, L., Stehle, P., Hellwig, P., Weber, S., and Schleicher, E. (2015) Spectroscopic Characterization of Radicals and Radical Pairs in Fruit Fly Cryptochrome - Protonated and Nonprotonated Flavin Radical-States. *FEBS J. 282* (16), 3175−3189.
(83) Chandrasekaran, S., Schneps, C. M., Dunleavy, R., Lin, C., DeOliveira, C. C., Ganguly, A., and Crane, B. R. (2021) Tuning Flavin Environment to Detect and Control Light-Induced Conformational Switching in Drosophila Cryptochrome. *Commun. Biol. 4* (1), 249.
(84) Vaidya, A. T., Chen, C. H., Dunlap, J. C., Loros, J. J., and Crane, B. R. (2011) Structure of a Light-Activated LOV Protein Dimer That Regulates Transcription. *Sci. Signaling 4* (184), No. ra50.
(85) Shu, X., Lev-Ram, V., Deerinck, T. J., Qi, Y., Ramko, E. B., Davidson, M. W., Jin, Y., Ellisman, M. H., and Tsien, R. Y. (2011) A Genetically Encoded Tag for Correlated Light and Electron Microscopy of Intact Cells, Tissues, and Organisms. *PLoS Biol. 9* (4), e1001041.
(86) Westberg, M., Bregnhøj, M., Etzerodt, M., and Ogilby, P. R. (2017) No Photon Wasted: An Efficient and Selective Singlet Oxygen Photosensitizing Protein. *J. Phys. Chem. B 121* (40), 9366−9371.
(87) Westberg, M., Etzerodt, M., and Ogilby, P. R. (2019) Rational Design of Genetically Encoded Singlet Oxygen Photosensitizing Proteins. *Curr. Opin. Struct. Biol. 57*, 56−62.
(88) Consiglieri, E., Xu, Q., Bregnhøj, M., Westberg, M., Ogilby, P. R., and Losi, A. (2019) Single Mutation in a Novel Bacterial LOV

Protein Yields a Singlet Oxygen Generator. *Photochem. Photobiol. Sci.* *18* (11), 2657−2660.
(89) Pimenta, F. M., Jensen, R. L., Breitenbach, T., Etzerodt, M., and Ogilby, P. R. (2013) Oxygen-Dependent Photochemistry and Photophysics of "MiniSOG," a Protein-Encased Flavin. *Photochem. Photobiol. 89* (5), 1116−1126.
(90) Westberg, M., Holmegaard, L., Pimenta, F. M., Etzerodt, M., and Ogilby, P. R. (2015) Rational Design of an Efficient, Genetically Encodable, Protein-Encased Singlet Oxygen Photosensitizer. *J. Am. Chem. Soc. 137* (4), 1632−1642.
(91) Rodríguez-Pulido, A., Cortajarena, A. L., Torra, J., Ruiz-González, R., Nonell, S., and Flors, C. (2016) Assessing the Potential of Photosensitizing Flavoproteins as Tags for Correlative Microscopy. *Chem. Commun. 52* (54), 8405−8408.
(92) Chen, C.-H., DeMay, B. S., Gladfelter, A. S., Dunlap, J. C., and Loros, J. J. (2010) Physical Interaction between VIVID and White Collar Complex Regulates Photoadaptation in Neurospora. *Proc. Natl. Acad. Sci. U. S. A. 107* (38), 16715−16720.
(93) Mathes, T., Vogl, C., Stolz, J., and Hegemann, P. (2009) In Vivo Generation of Flavoproteins with Modified Cofactors. *J. Mol. Biol. 385* (5), 1511−1518.
(94) Rinaldi, J., Gallo, M., Klinke, S., Paris, G., Bonomi, H. R., Bogomolni, R. A., Cicero, D. O., and Goldbaum, F. A. (2012) The *β*-Scaffold of the LOV Domain of the Brucella Light-Activated Histidine Kinase Is a Key Element for Signal Transduction. *J. Mol. Biol. 420* (1−2), 112−127.
(95) Snellenburg, J. J., Laptenok, S. P., Seger, R., Mullen, K. M., and van Stokkum, I. H. M. (2012) Glotaran: A Java -Based Graphical User Interface for the R Package TIMP. *Journal of Statistical Software 49* (3), 1−22.
(96) Brouwer, A. M. (2011) Standards for Photoluminescence Quantum Yield Measurements in Solution (IUPAC Technical Report). *Pure Appl. Chem. 83* (12), 2213−2228.
(97) Waterhouse, A., Bertoni, M., Bienert, S., Studer, G., Tauriello, G., Gumienny, R., Heer, F. T., De Beer, T. A. P., Rempfer, C., Bordoli, L., Lepore, R., and Schwede, T. (2018) SWISS-MODEL: Homology Modelling of Protein Structures and Complexes. *Nucleic Acids Res. 46* (W1), W296−W303.
(98) Zoltowski, B. D., Vaccaro, B., and Crane, B. R. (2009) Mechanism-Based Tuning of a LOV Domain Photoreceptor. *Nat. Chem. Biol. 5* (11), 827−834.
(99) Grosdidier, A., Zoete, V., and Michielin, O. (2011) SwissDock, a Protein-Small Molecule Docking Web Service Based on EADock DSS. *Nucleic Acids Res. 39* (Suppl.2), W270−W277.
(100) Horn, H. W., Swope, W. C., and Pitera, J. W. (2005) Characterization of the TIP4P-Ew Water Model: Vapor Pressure and Boiling Point. *J. Chem. Phys. 123* (19), 194504.
(101) Darden, T., York, D., and Pedersen, L. (1993) Particle Mesh Ewald: An N·log(N) Method for Ewald Sums in Large Systems. *J. Chem. Phys. 98* (12), 10089−10092.
(102) Ryckaert, J. P., Ciccotti, G., and Berendsen, H. J. C. (1977) Numerical Integration of the Cartesian Equations of Motion of a System with Constraints: Molecular Dynamics of n-Alkanes. *J. Comput. Phys. 23* (3), 327−341.
(103) Berendsen, H. J. C., Postma, J. P. M., Van Gunsteren, W. F., Dinola, A., and Haak, J. R. (1984) Molecular Dynamics with Coupling to an External Bath. *J. Chem. Phys. 81* (8), 3684−3690.
(104) Ganguly, A., Weissman, B. P., Giese, T. J., Li, N. S., Hoshika, S., Rao, S., Benner, S. A., Piccirilli, J. A., and York, D. M. (2020) Confluence of Theory and Experiment Reveals the Catalytic Mechanism of the Varkud Satellite Ribozyme. *Nat. Chem. 12* (2), 193−201.
(105) Lee, T. S., Cerutti, D. S., Mermelstein, D., Lin, C., Legrand, S., Giese, T. J., Roitberg, A., Case, D. A., Walker, R. C., and York, D. M. (2018) GPU-Accelerated Molecular Dynamics and Free Energy Methods in Amber18: Performance Enhancements and New Features. *J. Chem. Inf. Model. 58* (10), 2043−2050.
(106) Salomon-Ferrer, R., Götz, A. W., Poole, D., Le Grand, S., and Walker, R. C. (2013) Routine Microsecond Molecular Dynamics Simulations with AMBER on GPUs. 2. Explicit Solvent Particle Mesh Ewald. *J. Chem. Theory Comput. 9* (9), 3878−3888.
(107) Cornell, W. D., Cieplak, P., Bayly, C. I., Gould, I. R., Merz, K. M., Ferguson, D. M., Spellmeyer, D. C., Fox, T., Caldwell, J. W., and Kollman, P. A. (1995) A Second Generation Force Field for the Simulation of Proteins, Nucleic Acids, and Organic Molecules. *J. Am. Chem. Soc. 117* (19), 5179−5197.
(108) Roe, D. R., and Cheatham, T. E. (2013) PTRAJ and CPPTRAJ: Software for Processing and Analysis of Molecular Dynamics Trajectory Data. *J. Chem. Theory Comput. 9* (7), 3084−3095.
(109) Giambaşu, G. M., Luchko, T., Herschlag, D., York, D. M., and Case, D. A. (2014) Ion Counting from Explicit-Solvent Simulations and 3D-RISM. *Biophys. J. 106* (4), 883−894.
(110) Giambaşu, G. M., Gebala, M. K., Panteva, M. T., Luchko, T., Case, D. A., and York, D. M. (2015) Competitive Interaction of Monovalent Cations with DNA from 3D-RISM. *Nucleic Acids Res. 43* (17), 8405−8415.
(111) Giambaşu, G. M., Case, D. A., and York, D. M. (2019) Predicting Site-Binding Modes of Ions and Water to Nucleic Acids Using Molecular Solvation Theory. *J. Am. Chem. Soc. 141*, 2435−2445.
(112) Berendsen, H. J. C., Grigera, J. R., and Straatsma, T. P. (1987) The Missing Term in Effective Pair Potentials. *J. Phys. Chem. 91* (24), 6269−6271.
(113) Song, S. H., Madsen, D., Van Der Steen, J. B., Pullman, R., Freer, L. H., Hellingwerf, K. J., and Larsen, D. S. (2013) Primary Photochemistry of the Dark- and Light-Adapted States of the YtvA Protein from Bacillus subtilis. *Biochemistry 52* (45), 7951−7963.
(114) He, T.-F., Guo, L., Guo, X., Chang, C.-W., Wang, L., and Zhong, D. (2013) Femtosecond Dynamics of Short-Range Protein Electron Transfer in Flavodoxin. *Biochemistry 52* (51), 9120−9128.
(115) Mishra, B., Sharma, A., Naumov, S., and Priyadarsini, K. I. (2009) Novel Reactions of One-Electron Oxidized Radicals of Selenomethionine in Comparison with Methionine. *J. Phys. Chem. B 113* (21), 7709−7715.
(116) Hondal, R. J., Marino, S. M., and Gladyshev, V. N. (2013) Selenocysteine in Thiol/Disulfide-Like Exchange Reactions. *Antioxid. Redox Signaling 18* (13), 1675−1689.
(117) Le, D. T., Liang, X., Fomenko, D. E., Raza, A. S., Chong, C. K., Carlson, B. A., Hatfield, D. L., and Gladyshev, V. N. (2008) Analysis of Methionine/Selenomethionine Oxidation and Methionine Sulfoxide Reductase Function Using Methionine-Rich Proteins and Antibodies against Their Oxidized Forms. *Biochemistry 47* (25), 6685−6694.
(118) Liang, X., Kaya, A., Zhang, Y., Le, D. T., Hua, D., and Gladyshev, V. N. (2012) Characterization of Methionine Oxidation and Methionine Sulfoxide Reduction Using Methionine-Rich Cysteine-Free Proteins. *BMC Biochem. 13* (1), 21.
(119) Schöneich, C. (2002) Redox Processes of Methionine Relevant to *β*-Amyloid Oxidation and Alzheimer's Disease. *Arch. Biochem. Biophys. 397* (2), 370−376.
(120) Assmann, A., Briviba, K., and Sies, H. (1998) Reduction of Methionine Selenoxide to Selenomethionine by Glutathione. *Arch. Biochem. Biophys. 349* (1), 201−203.
(121) Assmann, A., Bonifačić, M., Briviba, K., Sies, H., and Asmus, K. D. (2000) One-Electron Reduction of Selenomethionine Oxide. *Free Radical Res. 32* (4), 371−376.
(122) Krause, R. J., and Elfarra, A. A. (2009) Reduction of L-Methionine Selenoxide to Seleno-l-Methionine by Endogenous Thiols, Ascorbic Acid, or Methimazole. *Biochem. Pharmacol. 77* (1), 134−140.
(123) Lavine, T. F. (1947) The Formation, Resolution, and Optical Properties of the Diastereoisomeric Sulfoxides Derived from L-Methionine. *J. Biol. Chem. 169* (3), 477−491.
(124) Mataga, N., Chosrowjan, H., Shibata, Y., and Tanaka, F. (1998) Ultrafast Fluorescence Quenching Dynamics of Flavin Chromophores in Protein Nanospace. *J. Phys. Chem. B 102* (37), 7081−7084.

https://doi.org/10.1021/acs.biochem.1c00064
Biochemistry 2021, 60, 1148−1164

(125) Magerl, K., Stambolic, I., and Dick, B. (2017) Switching from Adduct Formation to Electron Transfer in a Light-Oxygen-Voltage Domain Containing the Reactive Cysteine. *Phys. Chem. Chem. Phys. 19* (17), 10808−10819.
(126) Van Den Berg, P. A. W., Van Hoek, A., Walentas, C. D., Perham, R. N., and Visser, A. J. W. G. (1998) Flavin Fluorescence Dynamics and Photoinduced Electron Transfer in Escherichia coli Glutathione Reductase. *Biophys. J. 74* (4), 2046−2058.
(127) Visser, A. J. W. G., Van Den Berg, P. A. W., Visser, N. V., Van Hoek, A., Van Den Burg, H. A., Parsonage, D., and Claiborne, A. (1998) Time-Resolved Fluorescence of Flavin Adenine Dinucleotide in Wild-Type and Mutant NADH Peroxidase. Elucidation of Quenching Sites and Discovery of a New Fluorescence Depolarization Mechanism. *J. Phys. Chem. B 102* (50), 10431−10439.
(128) Drössler, P., Holzer, W., Penzkofer, A., and Hegemann, P. (2003) Fluoresence Quenching of Riboflavin in Aqueous Solution by Methionin and Cystein. *Chem. Phys. 286*, 409−420.
(129) Van Stokkum, I. H. M., Larsen, D. S., and Van Grondelle, R. (2004) Global and Target Analysis of Time-Resolved Spectra. *Biochim. Biophys. Acta, Bioenerg. 1657* (2−3), 82−104.
(130) Chovancova, E., Pavelka, A., Benes, P., Strnad, O., Brezovsky, J., Kozlikova, B., Gora, A., Sustr, V., Klvana, M., Medek, P., Biedermannova, L., Sochor, J., and Damborsky, J. (2012) CAVER 3.0: A Tool for the Analysis of Transport Pathways in Dynamic Protein Structures. *PLoS Comput. Biol. 8* (10), e1002708.
(131) *The PyMOL Molecular Graphics System*, ver. 1.8 (2015) Schrödinger, LLC.
(132) Nash, A. I., McNulty, R., Shillito, M. E., Swartz, T. E., Bogomolni, R. A., Luecke, H., and Gardner, K. H. (2011) Structural Basis of Photosensitivity in a Bacterial Light-Oxygen-Voltage/ Helix-Turn-Helix (LOV-HTH) DNA-Binding Protein. *Proc. Natl. Acad. Sci. U. S. A. 108* (23), 9449−9454.
(133) Schwerdtfeger, C., and Linden, H. (2003) VIVID Is a Flavoprotein and Serves as a Fungal Blue Light Photoreceptor for Photoadaptation. *EMBO J. 22* (18), 4846−4855.
(134) Zoltowski, B. D., Schwerdtfeger, C., Widom, J., Loros, J. J., Bilwes, A. M., Dunlap, J. C., and Crane, B. R. (2007) Conformational Switching in the Fungal Light Sensor Vivid. *Science (Washington, DC, U. S.) 316* (5827), 1054−1057.
(135) Herman, E., Sachse, M., Kroth, P. G., and Kottke, T. (2013) Blue-Light-Induced Unfolding of the Jα Helix Allows for the Dimerization of Aureochrome-LOV from the Diatom Phaeodactylum tricornutum. *Biochemistry 52* (18), 3094−3101.
(136) Herman, E., and Kottke, T. (2015) Allosterically Regulated Unfolding of the A'α Helix Exposes the Dimerization Site of the Blue-Light-Sensing Aureochrome-Lov Domain. *Biochemistry 54* (7), 1484−1492.
(137) Ataka, K., Hegemann, P., and Heberle, J. (2003) Vibrational Spectroscopy of an Algal Phot-LOV1 Domain Probes the Molecular Changes Associated with Blue-Light Reception. *Biophys. J. 84* (1), 466−474.
(138) Immeln, D., Pokorny, R., Herman, E., Moldt, J., Batschauer, A., and Kottke, T. (2010) Photoreaction of Plant and DASH Cryptochromes Probed by Infrared Spectroscopy: The Neutral Radical State of Flavoproteins. *J. Phys. Chem. B 114* (51), 17155−17161.
(139) Bergo, V., Mamaev, S., Olejnik, J., and Rothschild, K. J. (2003) Methionine Changes in Bacteriorhodopsin Detected by FTIR and Cell-Free Selenomethionine Substitution. *Biophys. J. 84* (2), 960−966.
(140) Grunenberg, A., and Bougeard, D. (1987) Vibrational Spectra and Conformational Phase Transition of Crystalline L-Methionine. *J. Mol. Struct. 160* (1−2), 27−36.
(141) Luchko, T., Gusarov, S., Roe, D. R., Simmerling, C., Case, D. A., Tuszynski, J., and Kovalenko, A. (2010) Three-Dimensional Molecular Theory of Solvation Coupled with Molecular Dynamics in Amber. *J. Chem. Theory Comput. 6* (3), 607−624.
(142) Genheden, S., Luchko, T., Gusarov, S., Kovalenko, A., and Ryde, U. (2010) An MM/3D-RISM Approach for Ligand Binding Affinities. *J. Phys. Chem. B 114* (25), 8505−8516.
(143) Kopka, B., Magerl, K., Savitsky, A., Davari, M. D., Röllen, K., Bocola, M., Dick, B., Schwaneberg, U., Jaeger, K. E., and Krauss, U. (2017) Electron Transfer Pathways in a Light, Oxygen, Voltage (LOV) Protein Devoid of the Photoactive Cysteine. *Sci. Rep. 7* (1), 13346.
(144) Aubert, C., Vos, M. H., Mathis, P., Eker, A. P. M., and Brettel, K. (2000) Intraprotein Radical Transfer during Photoactivation of DNA Photolyase. *Nature 405*, 586−590.
(145) Okajima, K., Fukushima, Y., Suzuki, H., Kita, A., Ochiai, Y., Katayama, M., Shibata, Y., Miki, K., Noguchi, T., Itoh, S., and Ikeuchi, M. (2006) Fate Determination of the Flavin Photoreceptions in the Cyanobacterial Blue Light Receptor TePixD (Tll0078). *J. Mol. Biol. 363* (1), 10−18.
(146) Kraft, B. J., Masuda, S., Kikuchi, J., Dragnea, V., Tollin, G., Zaleski, J. M., and Bauer, C. E. (2003) Spectroscopic and Mutational Analysis of the Blue-Light Photoreceptor AppA: A Novel Photocycle Involving Flavin Stacking with an Aromatic Amino Acid. *Biochemistry 42* (22), 6726−6734.
(147) Pace, C. N., Horn, G., Hebert, E. J., Bechert, J., Shaw, K., Urbanikova, L., Scholtz, J. M., and Sevcik, J. (2001) Tyrosine Hydrogen Bonds Make a Large Contribution to Protein Stability. *J. Mol. Biol. 312* (2), 393−404.
(148) Frisell, W. R., Chung, C. W., and Mackenzie, C. G. (1959) Catalysis of Oxidation Coenzymes of Nitrogen Compounds in the Presence of Light. *J. Biol. Chem. 234* (5), 1297−1302.
(149) Enns, K., and Burgess, W. H. (1965) The Photochemical Splitting of Water by Riboflavin. *J. Am. Chem. Soc. 87* (8), 1822−1823.
(150) Ninnemann, H. (1982) Photoreduction of Cytochrome B557 of Partially Purified Neurospora Nitrate Reductase via Its Internal Flavin. *Photochem. Photobiol. 35* (3), 391−398.
(151) Christie, J. M., Hitomi, K., Arvai, A. S., Hartfield, K. A., Mettlen, M., Pratt, A. J., Tainer, J. A., and Getzoff, E. D. (2012) Structural Tuning of the Fluorescent Protein iLOV for Improved Photostability. *J. Biol. Chem. 287* (26), 22295−22304.
(152) Mitra, D., Yang, X., and Moffat, K. (2012) Crystal Structures of Aureochrome1 LOV Suggest New Design Strategies for Optogenetics. *Structure 20* (4), 698−706.
(153) Grewal, R. K., Mitra, D., and Roy, S. (2015) Mapping Networks of Light-Dark Transition in LOV Photoreceptors. *Bioinformatics 31* (22), 3608−3616.
(154) Zayner, J. P., Antoniou, C., and Sosnick, T. R. (2012) The Amino-Terminal Helix Modulates Light-Activated Conformational Changes in AsLOV2. *J. Mol. Biol. 419* (1−2), 61−74.
(155) Schleicher, E., Kowalczyk, R. M., Kay, C. W. M., Hegemann, P., Bacher, A., Fischer, M., Bittl, R., Richter, G., and Weber, S. (2004) On the Reaction Mechanism of Adduct Formation in LOV Domains of the Plant Blue-Light Receptor Phototropin. *J. Am. Chem. Soc. 126* (35), 11067−11076.
(156) Zhu, J., Mathes, T., Hontani, Y., Alexandre, M. T. A., Toh, K. C., Hegemann, P., and Kennis, J. T. M. (2016) Photoadduct Formation from the FMN Singlet Excited State in the LOV2 Domain of Chlamydomonas reinhardtii Phototropin. *J. Phys. Chem. Lett. 7* (21), 4380−4384.
(157) Bialas, C., Barnard, D. T., Auman, D. B., McBride, R. A., Jarocha, L. E., Hore, P. J., Dutton, P. L., Stanley, R. J., and Moser, C. C. (2019) Ultrafast Flavin/Tryptophan Radical Pair Kinetics in a Magnetically Sensitive Artificial Protein. *Phys. Chem. Chem. Phys. 21* (25), 13453−13461.
(158) Marian, C. M., Nakagawa, S., Rai-Constapel, V., Karasulu, B., and Thiel, W. (2014) Photophysics of Flavin Derivatives Absorbing in the Blue-Green Region: Thioflavins as Potential Cofactors of Photoswitches. *J. Phys. Chem. B 118* (7), 1743−1753.
(159) Interlandi, G. (2018) Destabilization of the von Willebrand Factor A2 Domain under Oxidizing Conditions Investigated by Molecular Dynamics Simulations. *PLoS One 13* (9), e0203675.
(160) Mulinacci, F., Capelle, M. A. H., Gurny, R., Drake, A. F., and Arvinte, T. (2011) Stability of Human Growth Hormone: Influence

of Methionine Oxidation on Thermal Folding. *J. Pharm. Sci. 100* (2), 451−463.
(161) Lockhart, C., Smith, A. K., and Klimov, D. K. (2019) Methionine Oxidation Changes the Mechanism of Aβ Peptide Binding to the DMPC Bilayer. *Sci. Rep. 9* (1), 5947.
(162) Jori, G., Galiazzo, G., Marzotto, A., and Scoffone, E. (1968) Dye-Sensitized Selective Photooxidation of Methioxine. *Biochim. Biophys. Acta, Protein Struct. 154* (1), 1−9.
(163) Luo, S., and Levine, R. L. (2009) Methionine in Proteins Defends against Oxidative Stress. *FASEB J. 23* (2), 464−472.
(164) Levine, R. L., Moskovitz, J., and Stadtman, E. R. (2000) Oxidation of Methionine in Proteins: Roles in Antioxidant Defense and Cellular Regulation. *IUBMB Life 50* (4−5), 301−307.
(165) Jacob, C., Giles, G. I., Giles, N. M., and Sies, H. (2003) Sulfur and Selenium: The Role of Oxidation State in Protein Structure and Function. *Angew. Chem., Int. Ed. 42* (39), 4742−4758.
(166) Aledo, J. C. (2019) Methionine in Proteins: The Cinderella of the Proteinogenic Amino Acids. *Protein Sci. 28* (10), 1785−1796.
(167) Glaser, C. B., and Li, C. H. (1974) Reaction of Bovine Growth Hormone with Hydrogen Peroxide. *Biochemistry 13* (5), 1044−1047.
(168) Cascone, O., Biscoglio de Jimenez Bonino, M. J., and Santome, J. A. (1980) Oxidation of Methionine Residues in Bovine Growth Hormone by Chloramine-T. *Int. J. Pept. Protein Res. 16*, 299−305.
(169) Morgan, R. S., Tatsch, C. E., Gushard, R. H., Mcadon, J. M., and Warme, P. K. (1978) Chains of Alternating Sulfur and π-Bonded Atoms in Eight Small Proteins. *Int. J. Pept. Protein Res. 11* (3), 209−217.
(170) Aledo, J. C., Cantón, F. R., and Veredas, F. J. (2015) Sulphur Atoms from Methionines Interacting with Aromatic Residues Are Less Prone to Oxidation. *Sci. Rep. 5*, 16955.
(171) Valley, C. C., Cembran, A., Perlmutter, J. D., Lewis, A. K., Labello, N. P., Gao, J., and Sachs, J. N. (2012) The Methionine-Aromatic Motif Plays a Unique Role in Stabilizing Protein Structure. *J. Biol. Chem. 287* (42), 34979−34991.
(172) Towns, J., Cockerill, T., Dahan, M., Foster, I., Gaither, K., Grimshaw, A., Hazlewood, V., Lathrop, S., Lifka, D., Peterson, G. D., Roskies, R., Scott, J. R., and Wilkins-Diehr, N. (2014) XSeDe: Accelerating Scientific Discovery. *Comput. Sci. Eng. 16* (5), 62−74.

https://doi.org/10.1021/acs.biochem.1c00064
Biochemistry 2021, 60, 1148−1164